51st AIAA Aerospace Sciences Meeting including the New Horizons Forum and Aerospace Exposition
07 - 10 January 2013, Grapevine (Dallas/Ft. Worth Region), Texas

AIAA 2013-0500

Measurement of Static and Dynamic Performance Characteristics of Electric Propulsion Systems

Aron J. Brezina[1] and Scott K. Thomas[2]
Wright State University, Dayton, OH, 45435

Today's unmanned aerial vehicles are being utilized by numerous groups around the world for various missions. Most of the smaller vehicles that have been developed use commercially-off-the-shelf parts, and little information about the performance characteristics of the propulsion systems is available in the archival literature. In light of this, the aim of the present research was to determine the performance of various small-scale propellers in the 4.0 to 6.0 inch diameter range driven by an electric motor. An experimental test stand was designed and constructed in which the propeller/electric motor was mounted in a wind tunnel for both static and dynamic testing. Both static and dynamic results from the present experiment were compared to those from previous studies. For static testing, the coefficient of thrust, the coefficient of propeller power, and the overall efficiency, defined as the ratio of the propeller output power to the electrical input power, were plotted versus the propeller rotational speed. For dynamic testing, the rotational speed of the propeller was held constant at regular intervals while the freestream airspeed was increased from zero to the windmill state. The coefficient of thrust, the coefficient of power, the propeller efficiency and the overall efficiency were plotted versus the advance ratio for various rotational speeds. The thrust and torque were found to increase with rotational speed, propeller pitch and diameter, and decrease with airspeed. Using the present data and data from the archival and non-archival sources, it was found that the coefficient of thrust increases with propeller diameter for square propellers where *D = P*. The coefficient of thrust for a family of propellers (same manufacturer and application) was found to have a good correlation from static conditions to the windmill state. While the propeller efficiency was well correlated for this family of propellers, the goodness of fit parameter was improved by modifying the propeller efficiency with *D*/*P*.

Nomenclature

A_{P}	=	propeller disk area, m^2
A_{WT}	=	wind tunnel test section area, m^2
$C_{0.75}$	=	propeller chord length at the 75% radius, m
C_{P}	=	coefficient of propeller power
C_{Q}	=	coefficient of torque
C_{T}	=	coefficient of thrust
D	=	propeller diameter, m
F_{D}	=	fixture drag, N
H	=	height of Pitot tube from bottom of wind tunnel, m
I	=	electrical motor current, Amperes
J	=	advance ratio
K_{V}	=	motor velocity constant, RPM/Volt
n	=	propeller rotational speed, rev/s
P	=	propeller pitch, m
P_{atm}	=	atmospheric pressure, Pa
P_{diff}	=	Pitot tube differential pressure, Pa
P_{e}	=	electrical input power, W
P_{P}	=	propeller output power, W

[1] Graduate Student, Department of Mechanical and Materials Engineering, AIAA Member
[2] Associate Professor, Department of Mechanical and Materials Engineering, AIAA Member

Q = torque, N-m
$R_{0.75}$ = propeller 75% radius, m
R = particular gas constant, J/(kg-K)
$\mathrm{Re}_{0.75}$ = Reynolds number at the 75% radius of the propeller
T = measured thrust, N
T' = corrected thrust, N
T_{atm} = atmospheric temperature, K
T_{ref} = reference temperature, K
V = electric motor voltage, Volts
V_∞ = free-stream velocity, m/s
V'_∞ = corrected free-stream velocity, m/s
V_{P} = propeller velocity, m/s
V_{T} = total velocity, m/s
W = wind tunnel test section width and height, m
Δ = uncertainty
η_{P} = propeller efficiency
η_{T} = overall propulsion system efficiency
μ = absolute viscosity, kg/(m-s)
μ_{ref} = reference absolute viscosity evaluated at T_{ref}, kg/(m-s)
ρ = density, kg/m^3
τ_4 = Glauert correction variable

I. Introduction

Interest in the performance of small propellers operating at low Reynolds numbers has grown recently. The aerospace industry has developed numerous unmanned aerial vehicles (UAVs) and has kept most of the data about the propulsion systems proprietary. Very little information is available in the archival literature about the performance characteristics of these motor and propeller combinations. The present research and others like it have aimed to gather and compare information about these small propulsion systems so that proper motor and propeller combinations can be selected for a given mission profile. Several papers were reviewed that relate directly to the present work and provide direction for the research.

Brandt and Selig[1] experimentally determined efficiency as well as coefficients of thrust and power for low Reynolds number propellers. The parametric ranges were as follows: Propeller diameter $9 \le D \le 11$ inches, propeller rotational speed $1500 \le n \le 7500$ RPM, and the incoming air velocity V'_∞ ranged from zero (static) to the windmill state of each propeller, i.e., that point at which the propeller generates zero thrust. A test stand was built inside the UIUC wind tunnel to measure thrust, torque, and propeller rotational speed. Freestream air velocity was measured using a Pitot tube and one of two differential pressure transducers depending on the airspeed range. Velocity corrections were applied to account for the change in upstream airspeed at the Pitot tube created by the propeller as well as the pressure change created by the fairing and the constriction of the propeller slipstream caused by the walls. In total, 79 propellers from four different manufacturers were tested to find the coefficient of thrust, the coefficient of power and the propeller efficiency, all of which were plotted against advance ratio. The designs of the propellers ranged from those for electric motors to those used for fuel-powered engines. For each test, the rotational speed of each propeller was fixed while the freestream airspeed was varied. Four different values of propeller rotational speed (n = 3000, 4000, 5000, and 6000 RPM) were tested for each of the propellers. The results show that the propeller efficiency increases with the propeller speed. This is primarily due to the increase in Reynolds number as the propeller spins faster. Overall, the propeller efficiency ranged from $28 \le \eta_{\mathrm{P}} \le 65\%$. The propellers were also tested statically, but the data is only available in the UIUC propeller database[2].

Gamble[3] designed an intricate LabVIEW program to automatically collect data and generate propeller performance plots. A dynamometer was constructed using beam-type load cells to measure thrust and torque. The development of the LabVIEW program was detailed as well as a procedure for carrying out the experiment. Propellers were tested for repeatability by performing identical experiments over several days with two identical propellers. The results primarily focus on the effect of the Reynolds number on thrust and power coefficients and efficiency versus advance ratio. Thrust versus velocity was compared for propellers with constant diameter and varying pitch. Lastly, advance ratio was modified by replacing diameter with pitch in the equation for advance ratio. The optimal advance ratio is shown using this technique. This allows for the optimal pitch of a model propeller to be

selected to achieve maximum efficiency. The diameter can then be chosen from plots of thrust versus velocity to produce the required thrust for the airframe.

Deters and Selig[4] performed static tests on smaller propellers ranging from $2.5 \leq D \leq 5$ inches in diameter. Static coefficients of thrust and power as well as the figure of merit (FOM $= C_{\mathrm{T}}^{3/2}/\sqrt{2}C_{\mathrm{P}}$, typically used to measure the efficiency of helicopters) using modified coefficients of thrust and power that use disk area and tip speed were determined experimentally using a test stand specifically designed to test this size range of propellers. It was noted that the figure of merit should only be used for comparison when the disk loading is the same. The test stand utilized a 0.3 kg load cell and a 25 oz-in torque transducer to measure thrust and torque, respectively. Propeller rotational speeds ranging from $2500 \leq n \leq 27{,}000$ RPM were measured using an infrared detector. The test stand is not shown photographically, but a basic schematic is given indicating the locations of the components and a fairing surrounding the load cell and torque transducer. Calibrations of the components were performed and data was collected using a data acquisition board. The geometry of each propeller was found using PropellerScanner software[5] to find the chord and twist distribution. This was used to calculate the Reynolds number at the 75% chord location. Results show that over the rotational speed range tested, the figure of merit remained fairly constant throughout the test. The results also show that a larger diameter propeller is more efficient than a smaller one, and a propeller with a lower pitch is more efficient than one with a higher pitch.

Ol et al.[6] took a more analytical approach to studying small propellers operating at low Reynolds numbers. Iterative methods were used to calculate the coefficient of thrust, the coefficient of torque, and the propeller efficiency using propeller momentum theory and blade-element methods. Propellers were discretized by cutting and tracing sections as well as digital scans. Leading and trailing edges were fitted to the UIUC propeller library so that the resulting analysis in XFOIL would successfully converge. The iterative process for thrust was dependent on the various Reynolds numbers across the propeller blade at a given rotational speed. Two separate experimental setups were constructed to compare the numerical results. Propellers in the $6 \leq D \leq 12$ inch range were tested in the Langley Research Center Basic Aerodynamics Research Tunnel (BART) and larger propellers in the $14 \leq D \leq 20$ inch range were tested in the AFRL Vertical Wind Tunnel (VWT). Two different efficiencies were studied: The first was the propulsive efficiency where propeller speed was held constant and the forces and moments were shown versus rotational speed and airspeed. Static tests were performed with the wind tunnel sides open to alleviate the induced airflow velocity inside the wind tunnel. Blockage corrections were applied to BART tests but not to VWT tests, since the tunnel diameter of the VWT was greater than five times the diameter of the propellers tested. Drag on the test stand was corrected by sweeping tunnel velocity and generating curve fits that were used to adjust the actual data. A large sensitivity to twist distribution was observed in the tests and the analysis. Ol et al. postulated that plots of torque coefficient versus advance ratio are sometimes misleading because they do not account for Reynolds number effects. It was also shown that when the ratio of diameter to pitch is scaled (10×10 to 12×12, for example) the experimental data fits together well within the bounds of error. Modifications to the dimensionless terms to factor in propeller pitch were presented, however more research was deemed necessary to apply this theory.

Corrigan and Altman[7] examined different methods for wind tunnel blockage corrections. These methods included the Glauert[8] correction as well as a correction by Hackett et al.[9].These methods were described in detail and their applications were shown. A wind tunnel experiment was designed and constructed to record the necessary variables to calculate total system efficiency, defined as propulsive efficiency divided by electrical efficiency. This is in contrast to other works that primarily explored propeller efficiency. The stand was constructed using a beam-type load cell and a reaction torque sensor. Three propellers (D = 10, 12, and 14 inches) were tested using different motors for each propeller. Static pressure taps were used on the wall of the wind tunnel test section to record the changes in pressure forward and behind the propeller disk plane for the velocity corrections. The Glauert method did not provide sufficient correction for large blockage conditions. The Hackett method yielded more correction at higher airspeeds and larger propeller diameters, but the method could not be validated and therefore further work was found to be necessary.

Merchant and Miller[10] performed dynamic tests on propellers in the $6 \leq D \leq 22$ inch range. A test stand was constructed to record propeller performance parameters, where the thrust and torque were collected by a combined thrust/torque cell. The load and torque cell was calibrated using dead weights in the axial (thrust) and transverse (torque) directions. Wind tunnel velocity was measured directly using a Pitot probe and a differential pressure transducer. Since the propellers were large compared to the test section, blockage corrections developed by Glauert[8] were applied to the results. Readings were taken at wind-off-zero conditions before and after each test. These values were then averaged and subtracted from the test data to account for zero drift and temperature effects. Data was collected at constant propeller rotational speeds and the wind tunnel velocity was varied to sweep through values of advance ratio. The results were compared to other works and were shown to be acceptable. The setup was also tested for variations in flow angularity. Pitch and yaw variations between −3 and +3 arc degrees were examined and it was

shown that only the coefficient of thrust was affected by a change in pitch. However, it was shown that pitch variations of −3 and +3 degrees yielded the same results, which indicated that the system was symmetric in the pitch direction. Lastly, two identical propellers made by the same manufacturer were tested and compared, which showed that for some propellers there may be significant differences in performance due to manufacturing. Very limited results were presented, however, and the results shown only give a small sample of the entire test range.

The objective of the present research was to determine the performance of various commercially-available small-scale propellers driven by an electric motor. An experimental test stand was designed and constructed in which the electric motor was mounted in a wind tunnel at Wright State University for both static and dynamic testing. The freestream airspeed was varied from zero to the windmill state for each propeller. The rotational speed was varied over the operational range recommended by the propeller manufacturers, while ensuring that the electric motor did not overheat. The primary measurement devices were calibrated, and an extensive uncertainty analysis was performed. The results from the present experiment were compared to those from previous studies for both static and dynamic data. For static testing, the coefficient of thrust, the coefficient of propeller power, and the overall efficiency, defined as the propeller output compared to the electrical power input, were plotted versus the propeller rotational speed. For dynamic testing, the rotational speed of the propeller was held constant at regular intervals while the freestream airspeed was increased from zero to the maximum. The coefficient of thrust, the coefficient of power, the propeller efficiency and the overall efficiency were plotted versus the advance ratio for various rotational speeds.

II. Background

The performance characteristics to be determined by the experimental setup are as follows. The coefficients of thrust, torque, propeller power, and the propeller efficiency are:[10]

$$C_{\mathrm{T}} = \frac{T'}{\rho n^2 D^4} \tag{1}$$

$$C_Q = \frac{Q}{\rho n^2 D^5} \tag{2}$$

$$C_P = \frac{P_P}{\rho n^3 D^5} \tag{3}$$

$$\eta_{\mathrm{P}} = \frac{J C_{\mathrm{T}}}{C_{\mathrm{P}}} \tag{4}$$

The three performance coefficients and the propeller efficiency defined above are typically plotted against the advance ratio for dynamic testing:

$$J = \frac{V_\infty'}{nD} \tag{5}$$

where the corrected freestream velocity is:[8]

$$V_\infty' = V_\infty \left[1 - \frac{\tau_4 \left(\frac{A_{\mathrm{P}}}{A_{\mathrm{WT}}} \right)}{2\sqrt{1 + 2\tau_4}} \right] \tag{6}$$

The uncorrected freestream velocity is:

$$V_\infty = \sqrt{\frac{2P_{\mathrm{diff}}}{\rho}} \tag{7}$$

The Glauert correction variable is:

$$\tau_4 = \frac{T'}{\rho A_{\mathrm{P}} V_\infty^2} \tag{8}$$

The propeller disk area and wind tunnel area are, respectively:

$$A_{\mathrm{P}} = \frac{\pi D^2}{4}, \quad A_{\mathrm{WT}} = W^2 \tag{9}$$

The corrected thrust is defined as the measured thrust minus the drag force due to the flow of air over the motor, torque cell and load cell:[11]

$$T' = T - F_D \tag{10}$$

The overall propulsion system efficiency is the ratio of the propeller output power to the electrical input power:

$$\eta_{\mathrm{T}} = \frac{P_{\mathrm{P}}}{P_{\mathrm{e}}} = \frac{2\pi n Q}{VI} \tag{11}$$

The density of air is given by the perfect gas law:

$$\rho = \frac{P_{\mathrm{atm}}}{R T_{\mathrm{atm}}} \tag{12}$$

The Reynolds number at the 75% radius of the propeller is defined as follows for the static and dynamic tests:

$$\mathrm{Re}_{0.75,\mathrm{S}} = \frac{\rho V_{\mathrm{P}} C_{0.75}}{\mu}, \tag{13}$$

$$Re_{0.75,D} = \frac{\rho V_T C_{0.75}}{\mu} \tag{14}$$

where the propeller velocity and total velocity are given by:[10]

$$V_{\mathrm{P}} = 2\pi n R_{0.75}, \tag{15}$$

$$V_T = \sqrt{(V_\infty')^2 + V_P^2} \tag{16}$$

The absolute viscosity of air is a function of absolute temperature:[12]

$$\mu = \mu_{\mathrm{ref}} \left(\frac{T_{\mathrm{atm}}}{T_{\mathrm{ref}}} \right)^{0.76} \tag{17}$$

III. Experimental Setup

The objective of the present experiment was to determine the performance characteristics of small electric motor/propeller combinations from static conditions to the windmill state. Initially, a simple bench-top static test rig was designed and constructed to properly size the load cell and torque cell used in the experiment. The design, construction and test results from the bench-top static test rig are discussed in detail in the full thesis (Ref. 13).

The overall design of the dynamic test rig is shown in **Figure 2**. The electric motor was directly attached to a 25 oz-in torque cell (Transducer Techniques, Model RTS-25), which is able to withstand 10 kg in thrust and 1.7 kg in shear. The torque cell was in turn mounted onto a 1-kg single point beam-type load cell (Transducer Techniques, Model LSP-1). Each cell was driven by a signal conditioner (Transducer Techniques, Model TMO-1) that produced a 0 to 5 Volt linear output. The assembly of the motor, torque cell and load cell is shown in **Figure 1**. The motor is held in place with a custom-designed clam-shell clamp, in which fins were incorporated to increase the convective heat transfer from the electric motor to the air. This complex design was cut from a plate of 6061 aluminum using the wire electrical discharge machine (EDM) in the Micro Air Vehicle Lab at Wright State University.

The load cell was attached to a section of 1.25-inch square aluminum tubing, which acted as a riser to place the propeller in the middle of the test section. The bottom of the riser was connected to an optical breadboard table (Melles-Griot, Model BBSS-25-610-1219) using flanges of angle aluminum.

A hole was milled in the acrylic floor of the wind tunnel for the aluminum riser to pass through. The low-speed wind tunnel at Wright State University is an open circuit design capable of producing speeds from 0.6 to 36 m/s with a contraction ratio of 6.25:1. The square entrance of the wind tunnel has a 3.8 m^2 opening with an aluminum hexagonal honeycomb section that serves as a flow straightener. The height and width of the square test section is W = 0.6096 m, and its length is 2.438 m. Doors on one side of the test section allow for an entire wall to be opened for easy access. The diffuser is connected to an axial flow fan driven by a 20-hp electrical motor.

The data acquisition system used to collect data from the instrumentation consisted of a DAQ board (National Instruments, Model SCC-68) and a DAQ card (National Instruments, Model PCI-6221) installed in a PC. Shielded wires were used to connect the outputs of the transducers to the DAQ board. The electric motor driving the propeller was energized using a precision DC power supply (Hewlett-Packard, Model 6012B). A servo tester (GWS, Model MT-1) was used to control the rotational speed of the propeller[7]. The voltage supplied to the electric motor was measured using a digital multi-meter (National Instruments, Model USB-4065). To measure the current, a DC Hall effect current transducer (CR Magnetics, Model CR5210-30) with a range of 0 to 30 A was placed in-line between the power supply and the motor speed controller.

A remote optical sensor (Monarch Instrument, Model ROS-W) connected to a panel meter (Monarch Instrument, Model ACT-3X) was used to measure propeller rotational speed. Reflective tape supplied with the sensor was placed near the hub on the leeward side of the propeller so that the optical sensor did not have to be adjusted between runs. A roughly 5 × 5 mm piece of tape on each blade proved sufficient to get a good signal. The optical sensor was attached to the aluminum riser and aimed at the reflective tape.

Atmospheric pressure was measured to determine the density and absolute viscosity of the air. To record atmospheric pressure, a barometer (Vaisala, Model PTB110) capable of measuring 500 to 1100 mbar with accuracy of ±0.3 mbar was used. The differential pressure produced by the Pitot tube was measured using a differential pressure manometer (MKS, Model 226A) capable of reading a pressure differential of five Torr with an accuracy of 0.30% of the reading. The height of the Pitot tube from the floor of the wind tunnel was selected by traversing the boundary layer thickness using the Pitot tube as outlined in Appendix D of Ref. 13. The height was set to H = 2.5 inches, and the Pitot tube was made parallel to the wind tunnel walls by using a bubble level and a custom-made jig.

The temperature of the motor was measured using a Type T thermocouple while the temperature of the air inside the wind tunnel was measured using a Type E thermocouple probe (Omega, Model EMQSS-125G-12). The Type T thermocouple junction was placed on the center of the motor and held in place by the aluminum clam-shell clamp. Thermally conductive paste was placed on the thermocouple to aid in the transfer of heat. The Type E probe was mounted in the floor of the wind tunnel ahead of the motor/propeller so that the sensing junction extended into the airflow. The thermocouples were connected to thermocouple modules (National Instruments, Model SCC-TC01) on the data acquisition board. The signals from the eight sensors were read using custom-designed LabVIEW virtual instruments. The experimental data was reduced and tabulated using Excel.

The twenty-three propellers selected for analysis ranged from $4.0 \leq D \leq 6.0$ inches in diameter and $2.0 \leq P \leq 5.5$ inches in pitch. Some of the propellers were selected to overlap with previous research so that the procedures and test setup used for the measurements could be compared and validated. The GWS 4.5 × 3.0 and 5.0 × 4.3 inch propellers were tested statically and compared to Deters and Selig[4]. An APC 8.0 × 3.8 inch Slow Flyer was tested dynamically and compared to the results posted on the UIUC Propeller Database[2], while an APC 6.0 × 4.0 inch propeller was also tested dynamically and compared to the results presented by Ol et al.[6]. In order to accurately determine the diameter, 75% radius, and chord length at the 75% radius, three propellers of each type were measured using calipers. The three measurements for each of the propellers were then averaged and used in the calculations, as shown in Table 2, **Table 3**, and **Table 4**.

IV. Uncertainty Analysis

The uncertainties of all of the calculated results described in the above equations were determined using the root-sum-square uncertainty method[12]. Prior to conducting the experiments, three length measurements were made: Propeller diameter, D; propeller chord length at the 75% radius, $C_{0.75}$; and wind tunnel width, W. During experimentation, eight primary measurements were made using a data acquisition system: Uncorrected thrust, T; torque, Q; propeller rotational speed, n; atmospheric pressure, P_{atm}; atmospheric temperature, T_{atm}; Pitot tube pressure difference, P_{diff}; motor voltage, V; and motor amperage, I. The load cell, the torque cell, and the thermocouple used to measure the atmospheric temperature were calibrated in-house. In general, the calibration uncertainty is comprised of the uncertainty of the calibration standard and the difference between the prediction by the best-fit calibration line and the collected data point:

$$\Delta U_{\text{CAL}} = \Delta U_{\text{CS}} + |(mx + b) - U_{\text{DATA}}| \tag{18}$$

The measurement uncertainty can then be estimated to be the sum of the calibration uncertainty and the confidence interval of the collected data set at a confidence level of 99%:

$$\Delta U = \Delta U_{\text{CAL}} + \Delta U_{99} \tag{19}$$

The type E thermocouple probe used to measure the atmospheric temperature was calibrated over the anticipated ambient air temperature range in the wind tunnel room of 15 to 30°C in intervals of 5°C. In order to calibrate the torque cell, two identical arms were attached to the sides of the motor clamp so that the torque cell could be calibrated in both directions of rotation simultaneously. Varying weights were hung from one of the arms to calibrate in the clockwise direction, and then the process was repeated for the counterclockwise direction. The load cell used to measure thrust was calibrated in situ as follows. A strand of fishing line was attached to the front of the propeller using aircraft wire. This strand was then passed over a smooth cylinder with bearings mounted in the wind tunnel. Varying weights were suspended from the fishing line over the expected range of thrust.

The drag of the fixture was measured versus airspeed by removing the propeller and replacing it with just a propeller hub with the blades removed. The airspeed was increased systematically while data was collected from the load cell and the Pitot tube. The free-stream velocity was then calculated and the measured drag was plotted against the velocity. A second-order regression was applied to the points and this equation was used in the calculation of the corrected thrust.

Table 1 gives the uncertainties for each device or transducer used to collect the data. A complete discussion of the calibration process and a list of calibration certificates are given in Appendix A of Ref. 13. The principal equations used for determining the uncertainties of the computed quantities shown in the graphs in the Results and Discussion section are shown below. A complete listing of equations used is provided in Appendix B of Ref 13.

Coefficient of Thrust:

$$\Delta C_T = \left[\left(\frac{\Delta T}{\rho n^2 D^4}\right)^2 + \left(\frac{-T\Delta\rho}{\rho^2 n^2 D^4}\right)^2 + \left(\frac{-2T\Delta n}{\rho n^3 D^4}\right)^2 + \left(\frac{-4T\Delta D}{\rho n^2 D^5}\right)^2\right]^{\frac{1}{2}} \tag{20}$$

Coefficient of Torque:

$$\Delta C_Q = \left[\left(\frac{\Delta Q}{\rho n^2 D^5}\right)^2 + \left(\frac{-Q\Delta\rho}{\rho^2 n^2 D^5}\right)^2 + \left(\frac{-2Q\Delta n}{\rho n^3 D^5}\right)^2 + \left(\frac{-5Q\Delta D}{\rho n^2 D^6}\right)^2\right]^{\frac{1}{2}} \tag{21}$$

Coefficient of Power:

$$\Delta C_P = \left[\left(\frac{\Delta P_P}{\rho n^3 D^5}\right)^2 + \left(\frac{-P_P\Delta\rho}{\rho^2 n^3 D^5}\right)^2 + \left(\frac{-3P_P\Delta n}{\rho n^4 D^5}\right)^2 + \left(\frac{-5P_P\Delta D}{\rho n^3 D^6}\right)^2\right]^{\frac{1}{2}} \tag{22}$$

Propeller Efficiency:

$$\Delta\eta_{\mathrm{P}} = \left[\left(\frac{C_{\mathrm{T}}\Delta J}{C_{\mathrm{P}}}\right)^2 + \left(\frac{\Delta C_{\mathrm{T}} J}{C_{\mathrm{P}}}\right)^2 + \left(\frac{-JC_{\mathrm{T}}\Delta C_{\mathrm{P}}}{C_{\mathrm{P}}^2}\right)^2\right]^{\frac{1}{2}} \tag{23}$$

Advance Ratio:

$$\Delta J = \left[\left(\frac{\Delta V_\infty'}{nD}\right)^2 + \left(\frac{-V_\infty'\Delta n}{n^2 D}\right)^2 + \left(\frac{-V_\infty'\Delta D}{nD^2}\right)^2\right]^{\frac{1}{2}} \tag{24}$$

Overall Propulsion Efficiency:

$$\Delta\eta_{\mathrm{T}} = \left[\left(\frac{2\pi n\Delta Q}{VI}\right)^2 + \left(\frac{2\pi Q\Delta n}{VI}\right)^2 + \left(\frac{-2\pi nQ\Delta V_{\mathrm{e}}}{V^2 I}\right)^2 + \left(\frac{-2\pi nQ\Delta I}{VI^2}\right)^2\right]^{\frac{1}{2}} \tag{25}$$

Reynolds Number at 75% Propeller Radius (Static Testing):

$$\Delta\mathrm{Re}_{0.75,\mathrm{S}} = \left[\left(\frac{C_{0.75}V_{\mathrm{P}}\Delta\rho}{\mu}\right)^2 + \left(\frac{C_{0.75}\rho\Delta V_{\mathrm{P}}}{\mu}\right)^2 + \left(\frac{\rho V_{\mathrm{P}}\Delta C_{0.75}}{\mu}\right)^2 + \left(\frac{-C_{0.75}\rho V_{\mathrm{P}}\Delta\mu}{\mu^2}\right)^2\right]^{\frac{1}{2}} \tag{26}$$

Reynolds Number at 75% Propeller Radius (Dynamic Testing):

$$\Delta\mathrm{Re}_{0.75,\mathrm{D}} = \left[\left(\frac{C_{0.75}V_{\mathrm{t}}\Delta\rho}{\mu}\right)^2 + \left(\frac{C_{0.75}\rho\Delta V_{\mathrm{t}}}{\mu}\right)^2 + \left(\frac{\rho V_{\mathrm{t}}\Delta C_{0.75}}{\mu}\right)^2 + \left(\frac{-C_{0.75}\rho V_{\mathrm{t}}\Delta\mu}{\mu^2}\right)^2\right]^{\frac{1}{2}} \tag{27}$$

V. Test Procedures

In order to perform the experiments consistently, it was necessary to follow detailed procedures to collect data. Two separate procedures were developed for the static and dynamic tests. For all of the tests, the power supply driving the motor controller for the propeller motor was turned on and set to a nominal output of 11.1 Volts, which matches the voltage output of a standard 3-cell battery. Then, the data acquisition system and the signal conditioners driving the sensors were powered up for the warm-up periods recommended by the manufacturers. A file name and location were chosen in the data acquisition software that identified such parameters as propeller diameter, pitch, and propeller rotational speed. A complete description of the experimental procedures used is provided in Appendix E of Ref. 13.

A. Static Test Procedure

After the warm-up period, the load cell and torque cell were zeroed by adjusting the balance potentiometers on the signal conditioners so that the voltage outputs were as close as possible to zero. At this point, five hundred data points were collected with the propeller off in order to obtain a baseline for the actual value of zero for the load cell and torque cell. The propeller was then set to the first desired speed setting and one thousand data points were collected. The propeller was then turned off and another set of 500 data points was acquired. The average values for thrust and torque from the two propeller-off states were averaged and this value was used to correct the thrust and torque measurements to account for zero drift and temperature effects[10]. The process was then repeated for increased values of rotational speed until the maximum speed was achieved.

B. Dynamic Test Procedure

After the warm-up period, the differential pressure transducer reading the Pitot tube, the load cell, and the torque cell were zeroed. Five hundred data points were taken with the propeller motor off and the wind tunnel motor off. At

the end of the first five hundred points, the propeller motor was set to the desired rotational speed setting and the wind tunnel airspeed was set to the first desired setting. After the system reached steady state, one thousand data points were acquired. Next, the wind tunnel airspeed setting was changed and the propeller rotational speed was adjusted to match the original setting. This process was repeated until the windmill state of the propeller was reached. The propeller motor and the wind tunnel motor were both stopped at this point, and then five hundred data points were collected in order to again account for drift in the sensors. Data sets were collected for approximately ten wind tunnel airspeed settings for each of the four rotational speed settings for each propeller tested.

VI. Results and Discussion

To ensure that the collected data was repeatable and correct, tests were necessary to validate the static and dynamic results. The first type of test checked for repeatability of the same propeller as well as the repeatability across three identical propellers. The second type of test was to compare the results of the present experiment to published results from researchers using the same propeller. A complete summary of all of the data for the static and dynamic tests are provided in Appendix F and Appendix G of Ref. 13, respectively.

A. Validation of the Static Test

In order to check the repeatability of the experiment, three identical Graupner 4.7 × 4.7 inch propellers were tested under static conditions three times each, thus creating a total of nine sets of data. This was done to determine the repeatability of the experiment for multiple runs of the same propeller as well as establishing whether manufacturing variability affected the performance of identical propellers. Figure 3 shows typical results for a static propeller, where both the thrust and torque increase monotonically with rotational speed. Figure 4 shows that the repeatability of the reduced data (coefficient of thrust, coefficient of power and total efficiency) was excellent. The data from all nine tests fall within the uncertainty bounds for the first run. The duplicate propellers also fall directly in line, meaning that, at least for this type of propeller, manufacturing differences can be neglected. The uncertainties of the coefficients of thrust and power increased significantly at the lowest propeller rotational speed. This was driven by the uncertainty of the load cell and the torque cell at relatively small values of thrust and torque. Also, it was noted that at a rotational speed of n = 6000 rev/min, excessive vibrations were encountered, so that test was halted.

Static tests were performed on two propellers (GWS 4.5 × 3.0 and GWS 5.0 × 4.3) which matched tests performed by Deters and Selig[4]. The coefficient of thrust and the coefficient of power were compared to data provided by Deters and Selig as shown in Figure 5, where the results for both propellers show good agreement.

B. Static Test Results

Having established the validity of the experimental results, data was collected for all of the propellers shown in Table 2 - Table 4. Figure 6 shows a comparison between propellers with constant diameter and varying pitch, while Figure 7 gives a comparison between propellers with varying diameter and constant pitch. Each figure shows the coefficient of thrust, coefficient of power, and propeller efficiency. In Figure 6, the coefficients of thrust and power are relatively constant while the propeller efficiency increased with propeller rotational speed. The effect of reducing the pitch significantly decreased all three measures of performance. This same trend can be found in the data provided by Deters and Selig[4] for the coefficient of thrust and coefficient of power for the GWS 4.0 × 4.0 propeller versus that for the GWS 4.0 × 2.5 propeller. In Figure 7, the variation of the three performance parameters with varying propeller diameter is also shown to be significant, where increasing the diameter decreased the thrust coefficient and power coefficient but increased the propeller efficiency. This trend is also apparent in the data reported by Deters and Selig[4] for the following propellers: GWS 3.0 × 3.0, GWS 4.5 × 3.0, and GWS 5.0 × 3.0.

C. Validation of the Dynamic Test

The dynamic test procedure and experiment were validated similarly to the static experiment. Figure 8 shows typical dynamic results for the thrust and torque generated by one propeller over the full range of airspeed and various levels of rotational speed. Both the thrust and torque increase with rotational speed and decrease with airspeed, as expected. The APC 8.0 × 3.8 inch Slow Flyer propeller was tested at nominal propeller rotational speeds of n = 4000 and 7000 rpm, and the results for the coefficient of thrust, the coefficient of power, and the propeller efficiency versus advance ratio were compared to those reported on the UIUC propeller database[2], as shown in Figure 9. In general, the coefficient of thrust and coefficient of power decrease with advance ratio, whereas the propeller efficiency reaches a peak value, as shown in Figure 9(c). The agreement with the data from the UIUC

database is excellent for both rotational speeds, even where the propeller efficiency drops off steeply with advance ratio.

To further validate the dynamic results, an APC 6.0 × 4.0 inch propeller was tested at nominal propeller rotational speeds of n = 8000 to 16000 rpm by intervals of 2000 rpm and compared to the results for the coefficient of thrust, the coefficient of torque, and propeller efficiency versus advance ratio reported by Ol et al.[6], as shown in Figure 10. Again, the coefficients of thrust and torque decrease with advance ratio and the propeller efficiency increases to a peak and then decreases. Since the exact propeller rotational speed tested by Ol et al. is unclear, it can only be compared to the trends in the data. The present data agrees with that shown by Ol et al. and the trends are similar. At a rotational speed of n = 8000 rpm, the propeller was tested by sweeping the advance ratio from low to high values, and then sweeping from high to low values to examine the potential for hysteresis in the experiment. As can be seen, there is not a noticeable difference between these two sets of data.

D. Dynamic Test Results

With the dynamic results validated, data was collected for all of the propellers. Similarly to the static tests, comparisons were drawn between propellers with constant diameter and varying pitch in Figure 11 and between propellers with constant pitch and varying diameter in Figure 12, both at a nominal rotational speed of n = 16000 rpm. In Figure 11, propellers with larger pitch generally had larger coefficients of thrust and power, and the windmill state occurred at higher values of the advance ratio, which indicates that larger pitch values tend to allow for higher airspeed. The results for the propeller efficiency given in Figure 11(c) shows that the efficiency decreases with increasing pitch for lower values of advance ratio, and the peak efficiency occurs at higher values of advance ratio. An increase in pitch essentially means that the angle of attack of the airfoil is higher, which should increase both thrust and torque prior to reaching stall. In Figure 12, increasing the propeller diameter for a given pitch tends to decrease the coefficient of thrust and the coefficient of power, and the propeller efficiency increases with diameter for lower values of advance ratio. Increasing the diameter for a given rotational speed and airspeed actually increases the thrust and torque due to the increased wingspan of the propeller, but this effect is negated due to the factor of D4 in the denominator of C_T and the factor of D^5 in the denominator of the C_P.

Figure 13 presents results for square propellers, where D = P, from Ol et al.[6], Selig[2], and the present experiment for a fairly wide range in propeller diameter ($4.0 \leq D \leq 18$ inches). Ol et al. had conjectured that the coefficient of thrust should collapse for square propellers. The results are grouped from small to large propeller diameter, where the three researchers essentially covered different diameter ranges. In general, the coefficient of thrust appears to increase with diameter, but more data would be required to make a definitive statement.

Figure 14 presents the coefficient of thrust for the same family of APC propellers (Speed 400 Electric). In this case, the diameter to pitch ratio for this group of propellers has a relatively small range ($0.86 \leq D/P \leq 1.5$). However, it was found that the other types of propellers (Free Flight, Sport, Thin Electric, Slow Flyer) have noticeably different blade shapes, which could induce variations in the results simply due to the geometry of the propeller which could not be accounted for by using D/P alone. Figure 14(a) shows the coefficient of thrust versus advance ratio for all of the collected data for the APC Speed 400 Electric propellers with an uncertainty level of $\Delta C_T \leq 20\%$. As can be seen, the results are not correlated well, as witnessed by the low goodness of fit parameter, $R^2 = 0.539$. As the uncertainty requirement becomes more restrictive, less data points are permitted to be graphed, which should increase the accuracy of the predictive best-fit line. However, this in itself becomes problematic, since more data points (for the $\Delta C_T = 20\%$ case, for example) would provide more confidence in the resulting best-fit line. It is entirely possible that, if the uncertainty requirement should become too restrictive, the best-fit line could become erratic due to an insufficient number of data points. Conversely, if the uncertainty requirement becomes too lax, the accuracy of the predictive curve would suffer due to inclusion of obviously erroneous data points. It should be noted that many of the data points near the windmill state, where the thrust approaches zero, will not appear in these graphs due to the fact that the values of thrust are much lower than the uncertainty. Figure 14(b) shows the coefficient of thrust modified by D/P plotted against advance ratio. This change to coefficient of thrust improves the goodness of fit parameter to $R^2 = 0.680$. This gives a better correlation than (a) but this can be improved by modifying the advance ratio by D/P as seen in Figure 14(c). This improves the goodness of fit parameter to a value of $R^2 = 0.720$. This is a large improvement over the original data and shows that the data fits together better when modified by the diameter to pitch ratio.

Figure 15(a) similarly shows the coefficient of power versus advance ratio for all of the collected data with an uncertainty level of $\Delta C_P \leq 20\%$. As can be seen, the results are not correlated well, as witnessed by the very low goodness of fit parameter, $R^2 = 0.059$. Figure 15(b) shows a coefficient of power that is modified by the diameter to pitch ratio squared, which improves the goodness of fit parameter to $R^2 = 0.538$. This is still relatively low, and probably should not be used in most engineering analyses. Figure 16 shows a similar comparison for the propeller

efficiency versus the advance ratio. Here, the diameter to pitch ratio was used to modify the original advance ratio to increase the goodness of fit parameter from $R^2 = 0.938$ to 0.983, which is deemed to be very accurate for most applications, especially for advance ratios less than $J \leq 0.4$, which is near the peak efficiency predicted by the best-fit curve.

VII. Conclusions

Twenty-three propellers in the range of $4.0 \leq D \leq 6.0$ inches in diameter and $2.0 \leq P \leq 5.5$ inches in pitch were tested statically and dynamically in the Wright State University wind tunnel over a wide range of propeller rotational speeds and air speeds. A detailed experimental procedure for both cases was employed and an extensive uncertainty analysis was performed on the resulting data. The experiments were validated by comparing the results to previous works. The repeatability of the experimental results and the repeatability of the manufacture of the propellers were proven by testing three duplicate propellers three times each. Static tests were performed by varying propeller speed from n = 4000 rpm to the maximum speed limited by the manufacturer's specifications or the maximum motor temperature. Dynamic tests were performed by holding the propeller speed constant and varying the wind tunnel airspeed and thus varying the advance ratio.

For a given airspeed and rotational speed, the thrust and torque both increased with propeller pitch and diameter, as expected. Propeller efficiencies ranged from 24% to 52% for some of the more efficient designs. It was found that the coefficient of thrust for square propellers, where D = P, increased with the propeller diameter. The coefficient of thrust for a family of propellers (same manufacturer and application) was found to have a good correlation that was well predicted over a range of diameter to pitch ratio of $0.86 \leq D/P \leq 1.5$. Results for different propeller manufacturers and even the same manufacturer with higher values of D/P did not correlate well, possibly due to variations of the propeller blade geometry that was not accounted for by D/P alone. The correlation of the coefficient of thrust versus advance ratio plot was improved by modifying both the coefficient of thrust and advance ratio by the diameter to pitch ratio. The coefficient of power for this family of propellers was not found to be well correlated by either the original definition of the coefficient, or with a power coefficient that was modified by D/P squared. The propeller efficiency of the above-mentioned set of propellers was plotted using the original expression for propeller efficiency versus advance ratio as well as a modified advance ratio, and it was determined that the correlation was improved substantially by using the modified advance ratio expression. The data reported here will serve to add to the database of work produced by others by filling in a critical range in propeller diameters previously untested dynamically. The results will provide future aircraft designers and researchers much needed information about the propellers and propulsion systems needed to create new aircraft designs or modifying existing designs.

Appendix

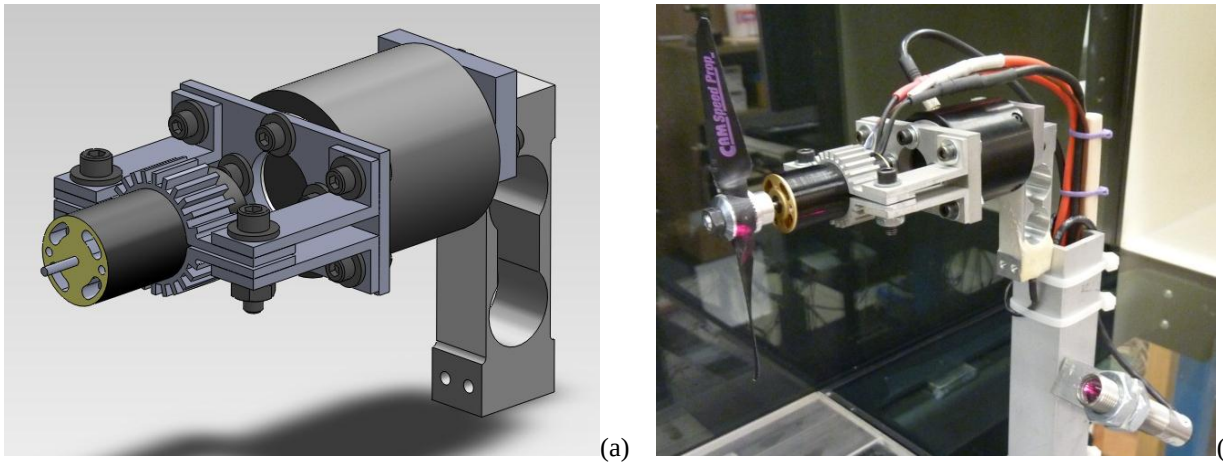

Figure 1. Assembly of Motor, Torque Cell and Load Cell: (a) Solid Model Representation; (b) Photograph.

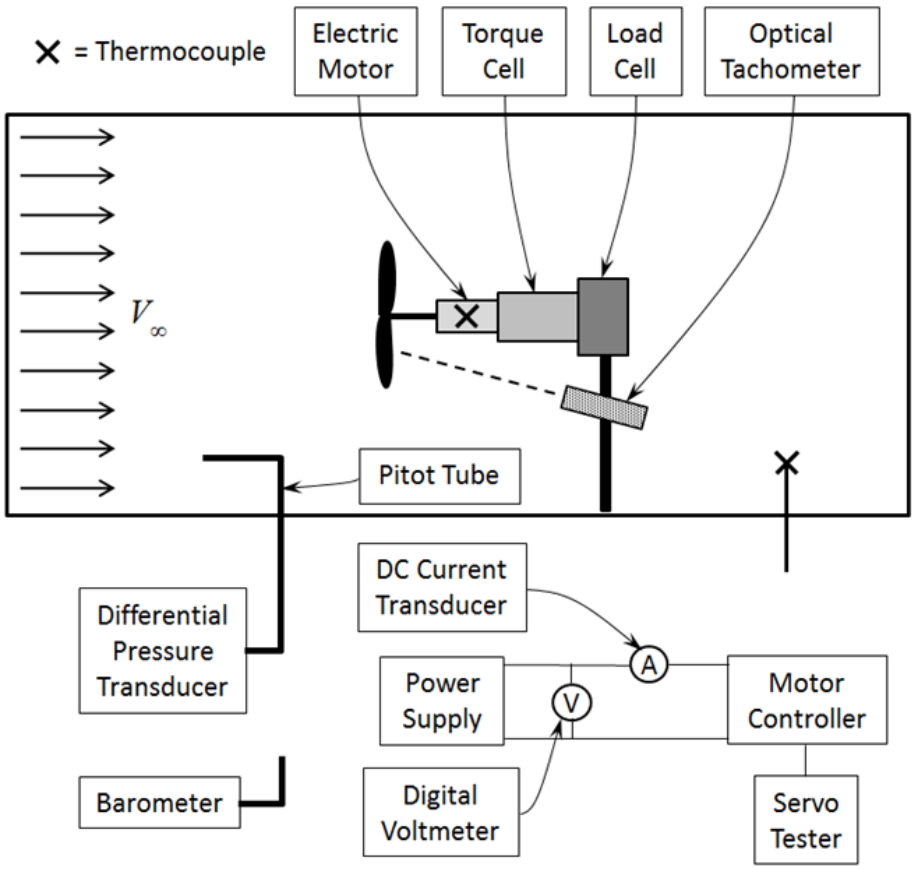

Figure 2. Schematic Diagram of the Experimental Setup.

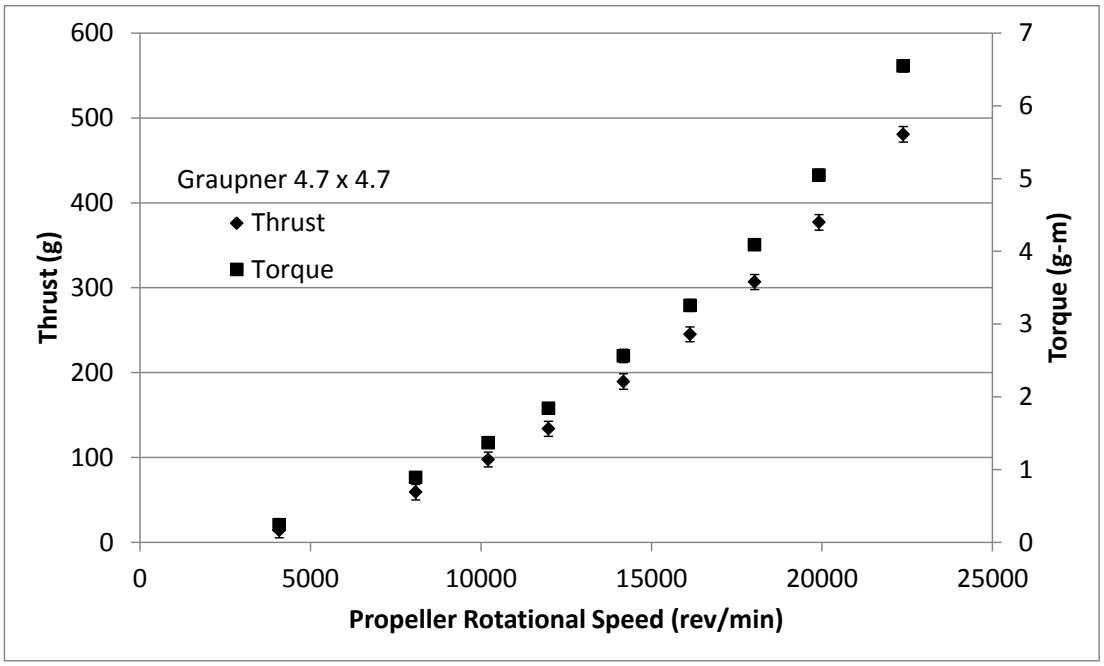

(a)

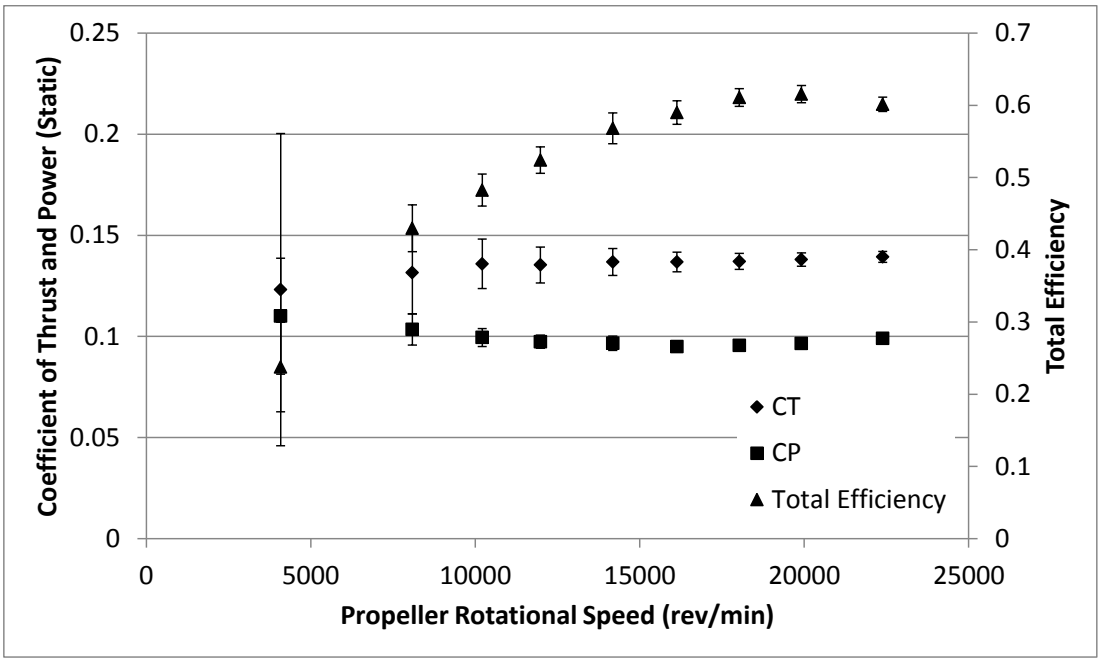

(b)

Figure 3. Typical Static Test Results (Graupner 4.7 × 4.7 inch Propeller): (a) Thrust and Torque Versus Rotational Speed, (b) Coefficient of Thrust, Power and Total Efficiency Versus Rotational Speed.

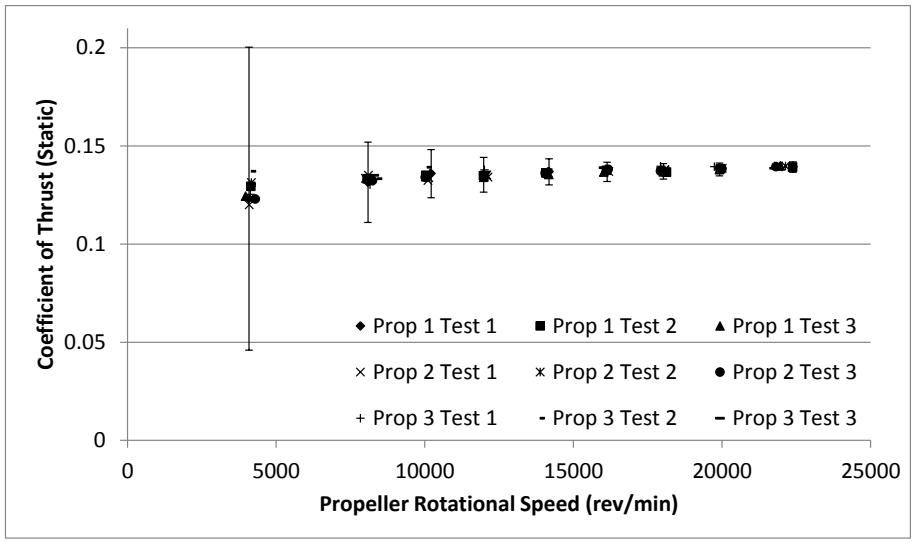

(a)

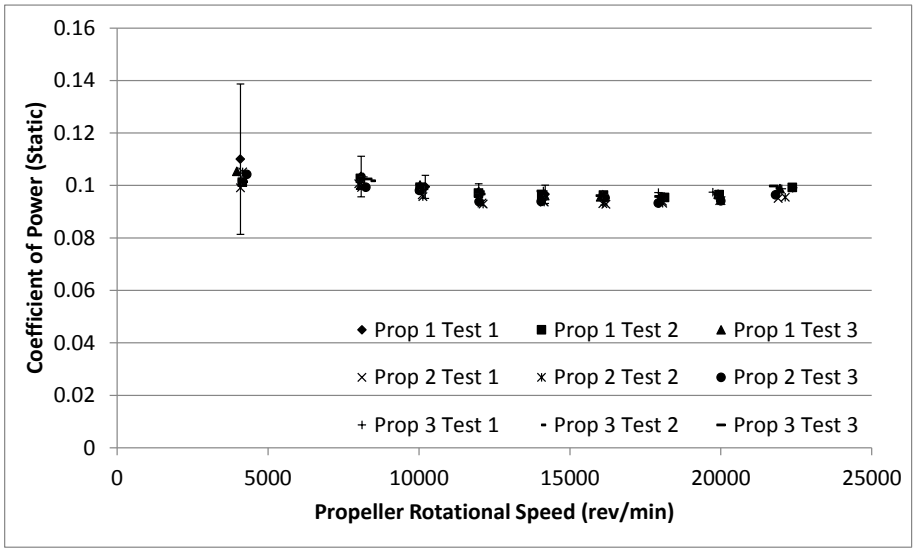

(b)

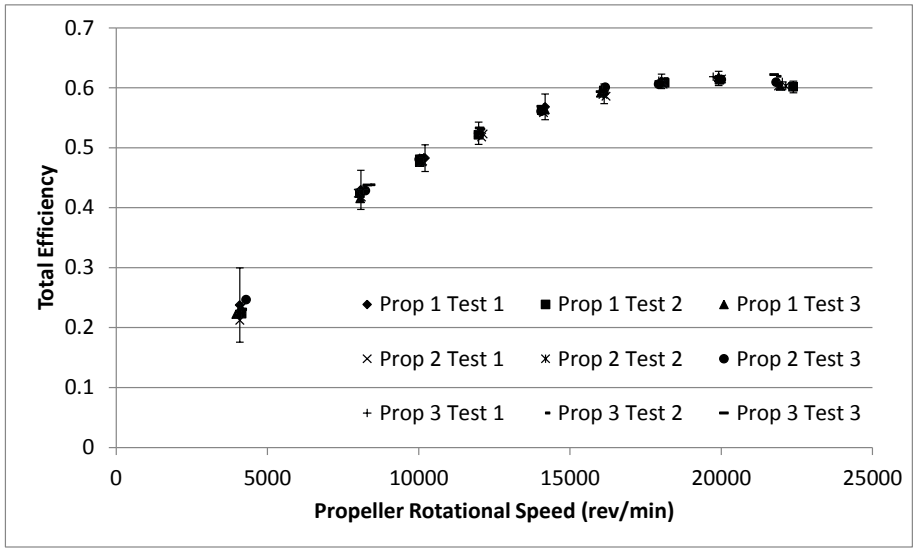

(c)

Figure 4. Comparison of Three Identical Propellers (Graupner 4.7 × 4.7): (a) Static Coefficient of Thrust, (b) Static Coefficient of Power, (c) Static Total Efficiency.

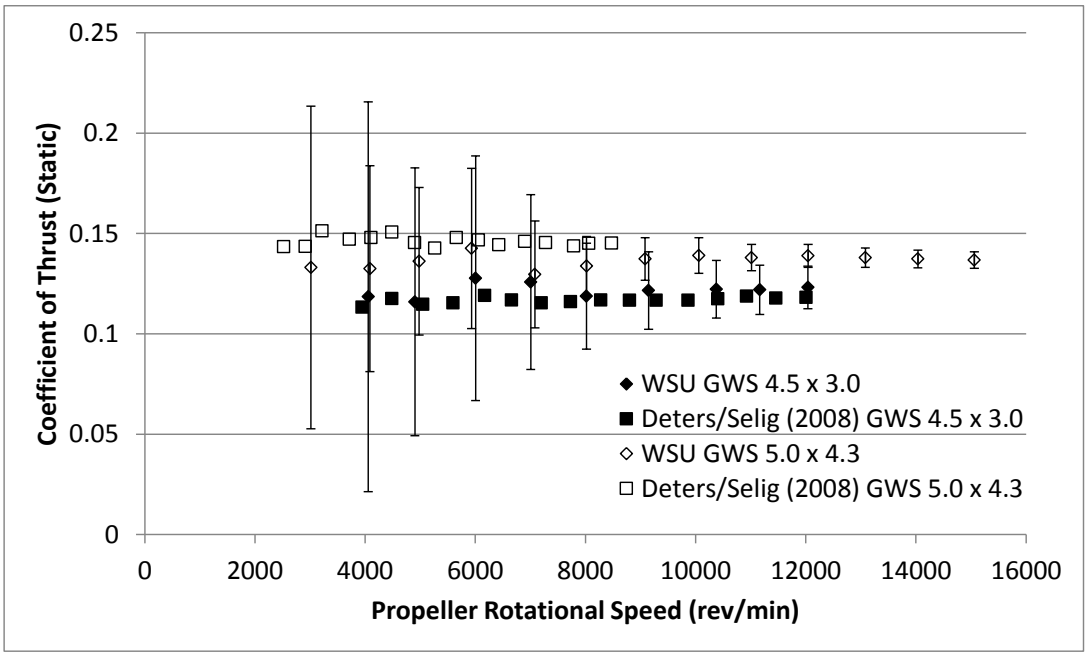

(a)

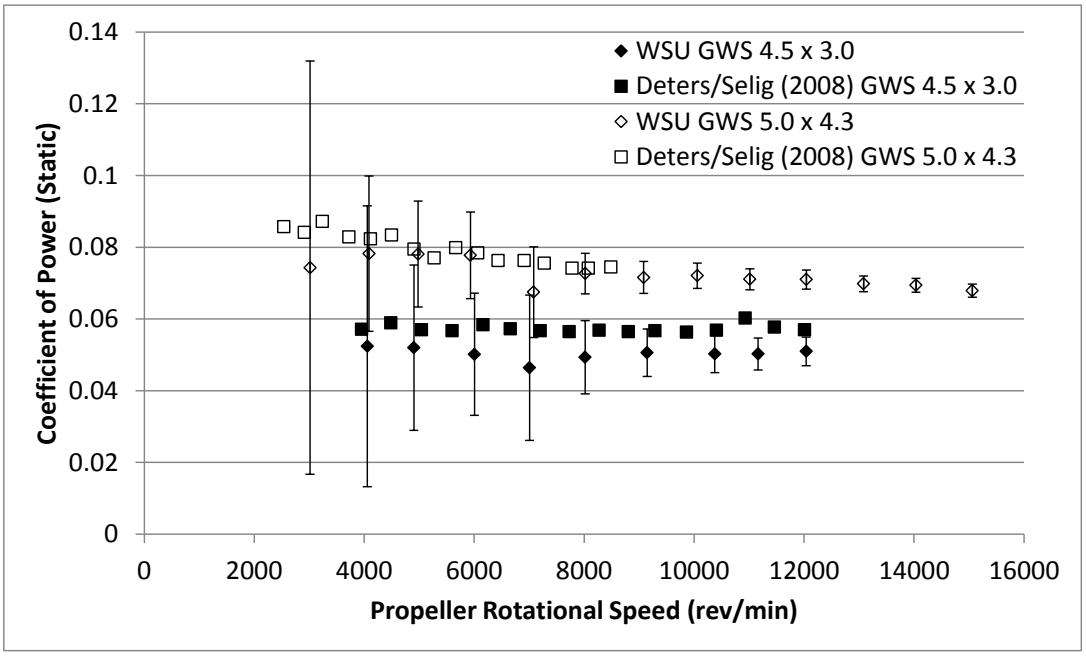

(b)

Figure 5. Comparison of the Present Results to Deters and Selig[4] (GWS 4.5 × 3.0 and GWS 5.0 × 4.3 Propellers): (a) Static Coefficient of Thrust, (b) Static Coefficient of Power.

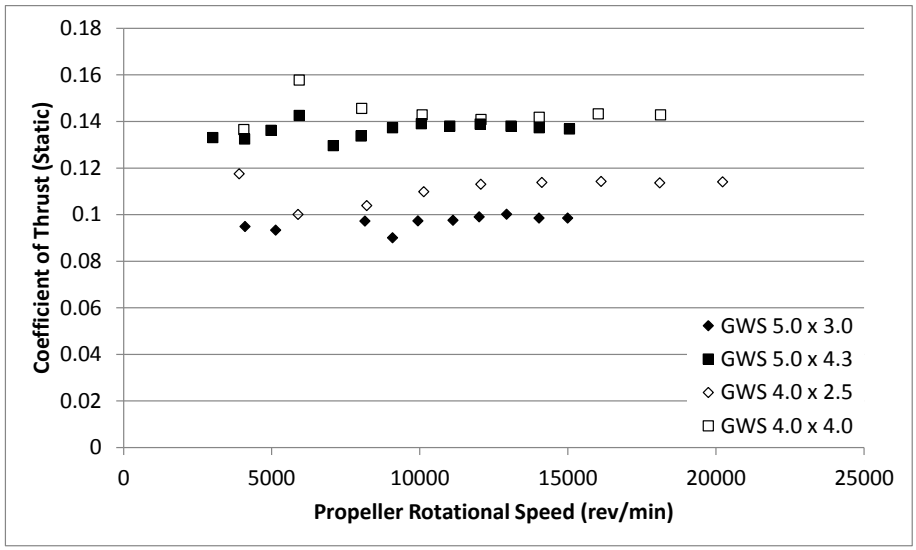

(a)

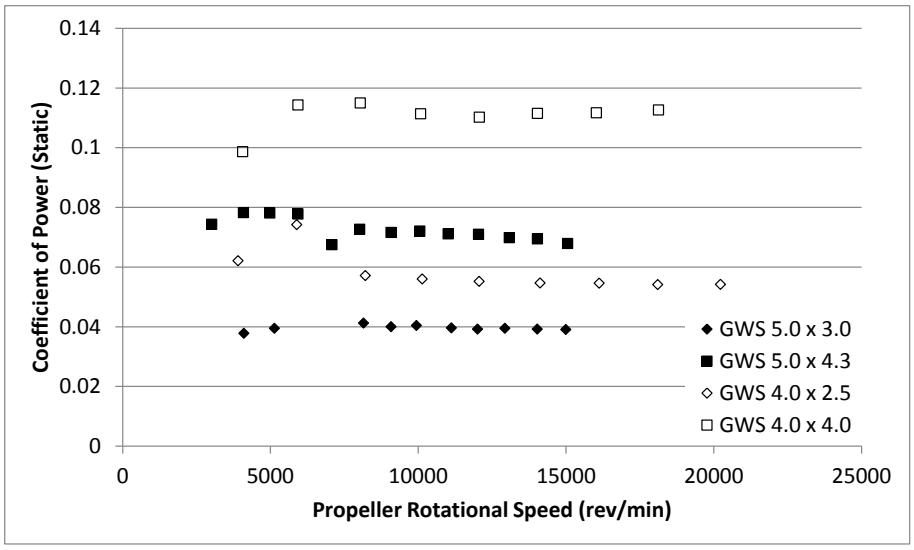

(b)

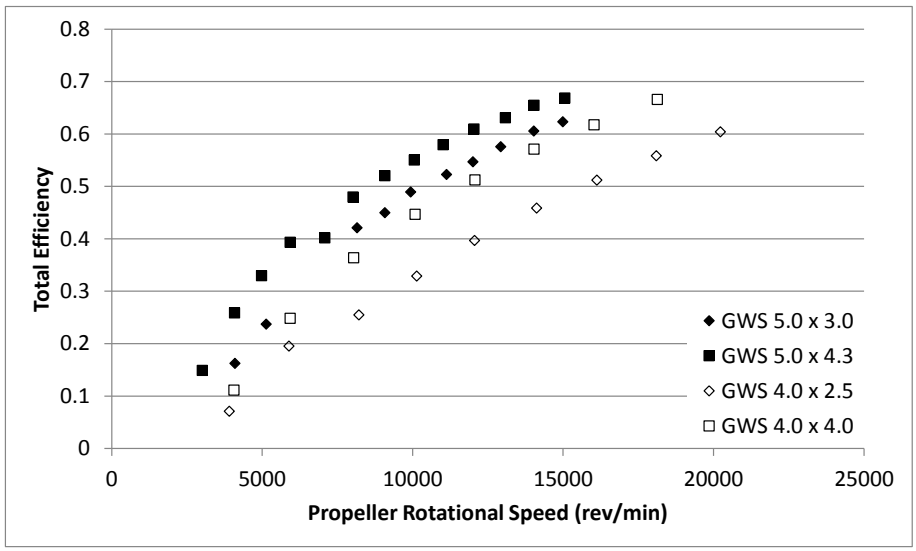

(c)

Figure 6. The Effect of Varying Propeller Pitch While Holding Diameter Constant: (a) Static Coefficient of Thrust, (b) Static Coefficient of Power, (c) Static Total Efficiency.

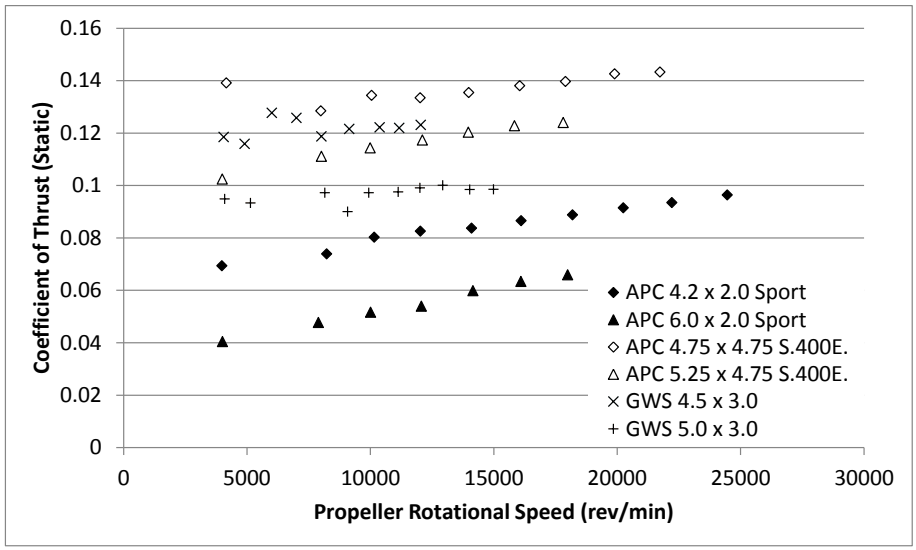

(a)

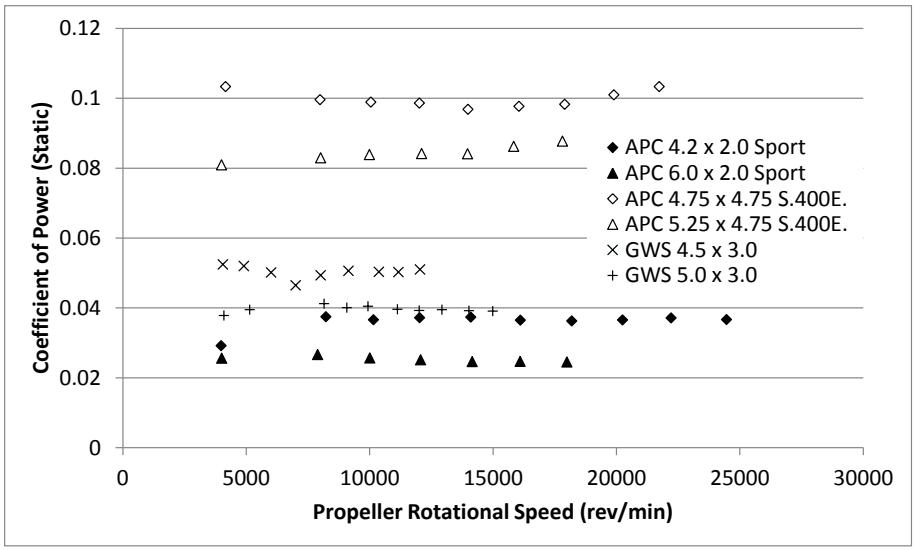

(b)

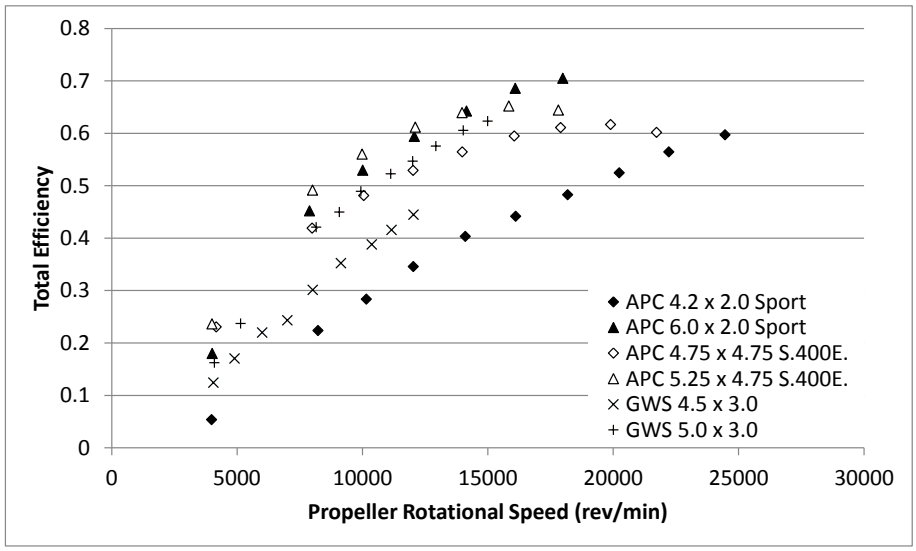

(c)

Figure 7. The Effect of Varying Propeller Diameter While Holding Pitch Constant: (a) Static Coefficient of Thrust, (b) Static Coefficient of Power, (c) Static Total Efficiency.

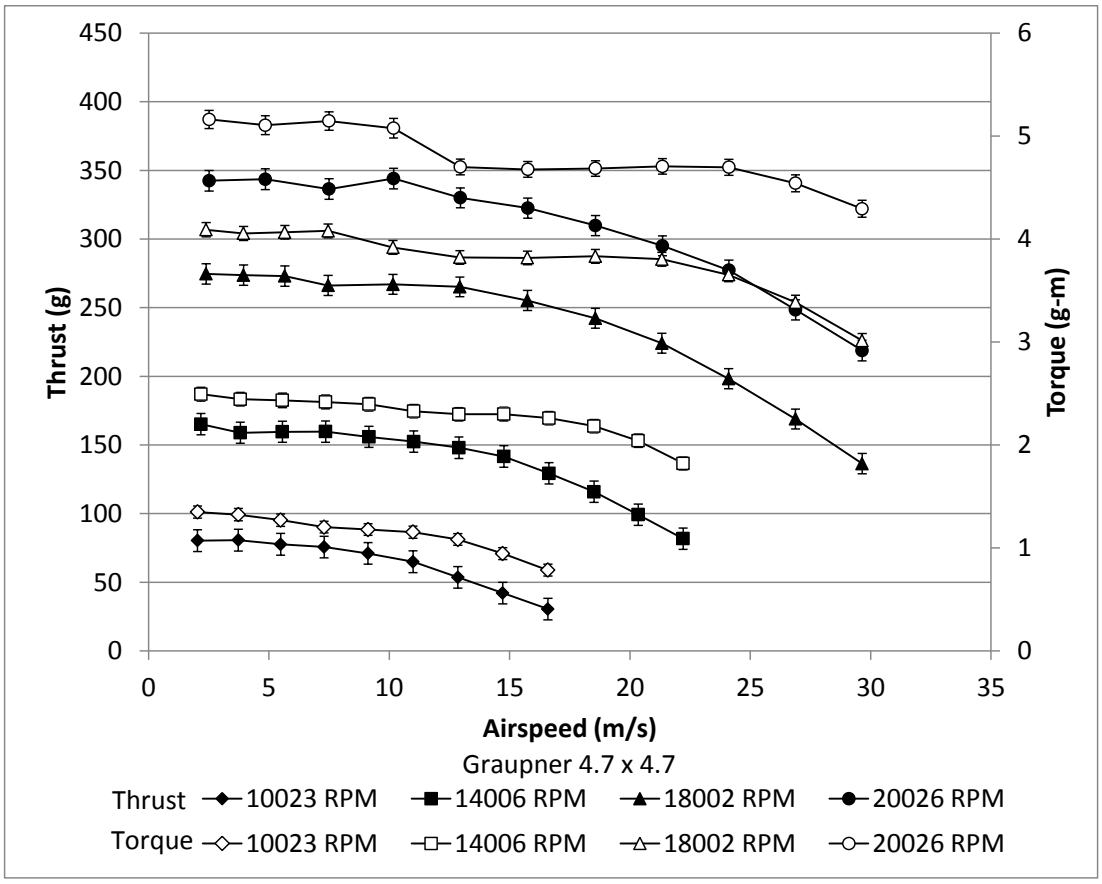

(a)

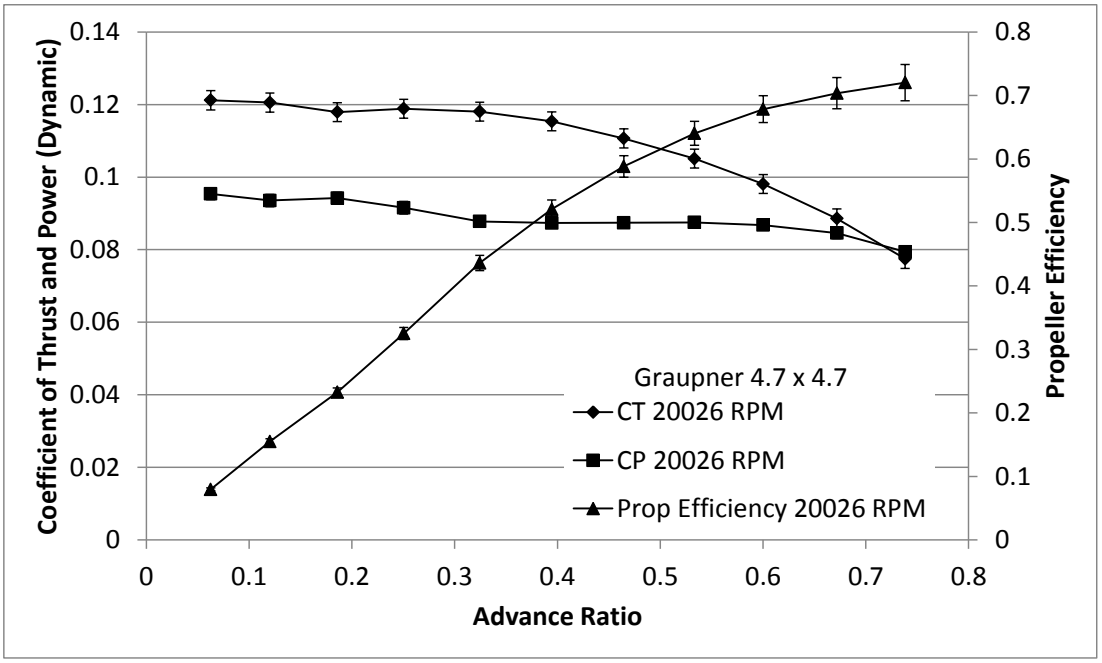

(b)

Figure 8. Typical Dynamic Test Results (Graupner 4.7 × 4.7 inch Propeller): (a)Thrust and Torque Versus Airspeed for Various Rotational Speeds, (b) Coefficient of Thrust, Power and Propeller Efficiency Versus Advance Ratio.

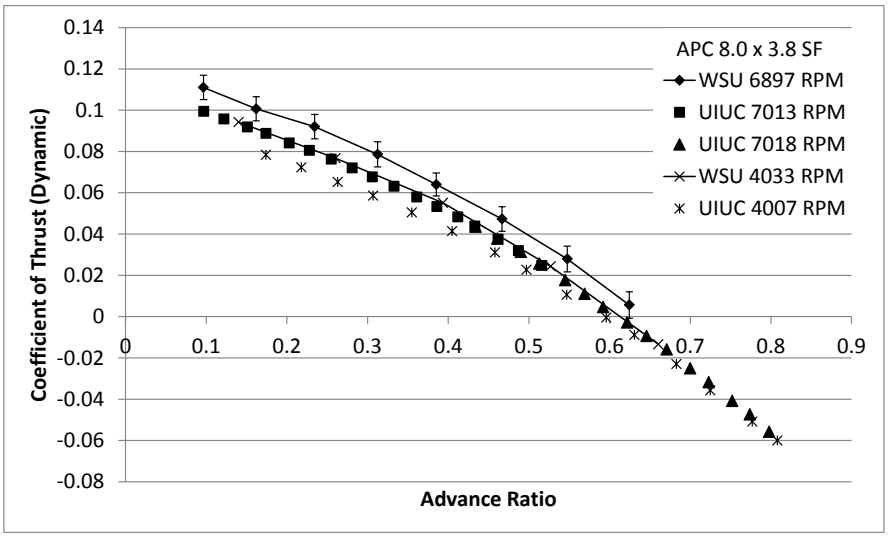

(a)

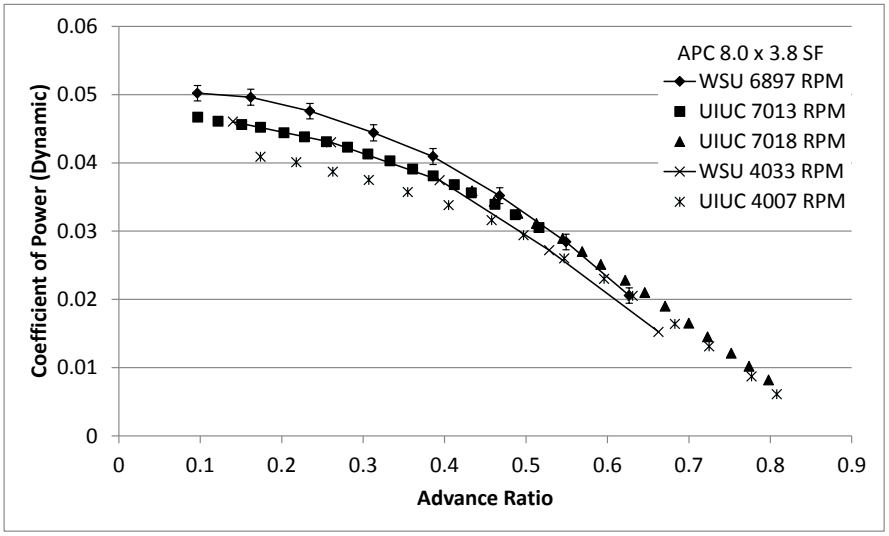

(b)

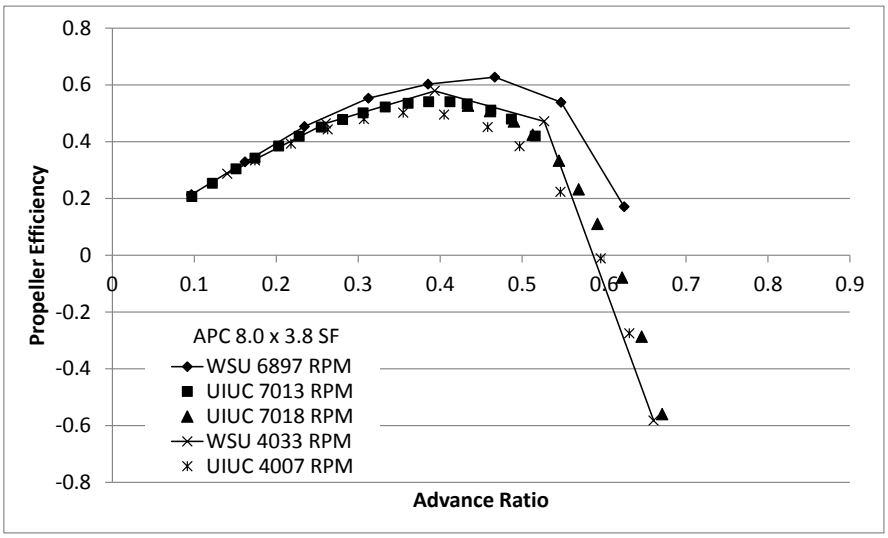

(c)

Figure 9. Comparison of Present Results to Selig[2] (APC 8.0 × 3.8 SF): (a) Dynamic Coefficient of Thrust, (b) Dynamic Coefficient of Power, (c) Propeller Efficiency.

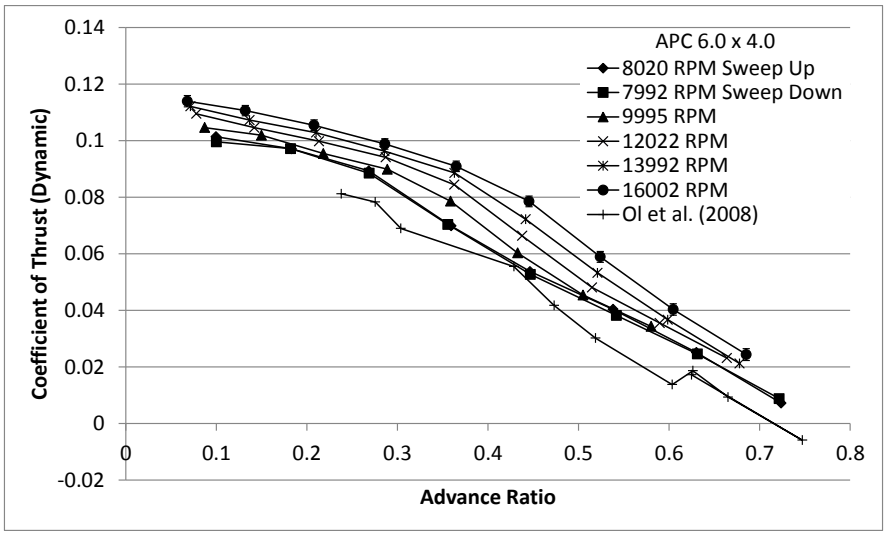

(a)

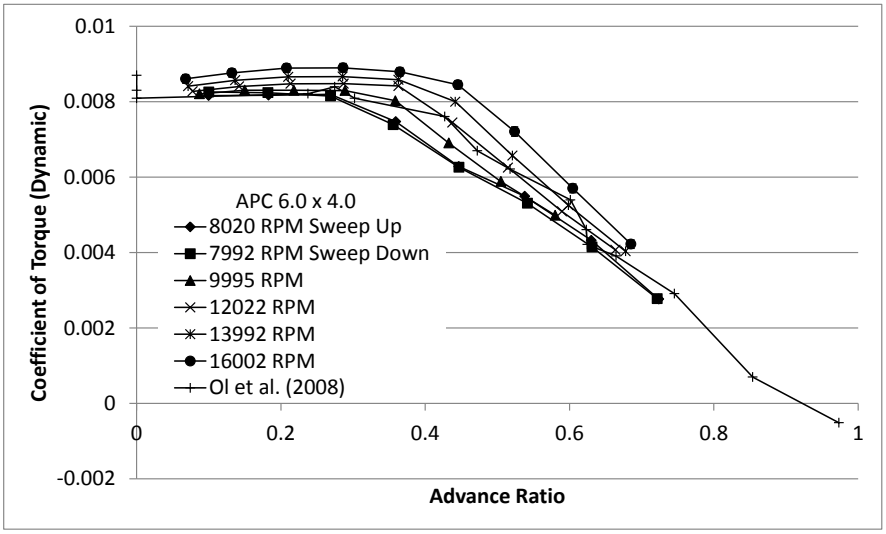

(b)

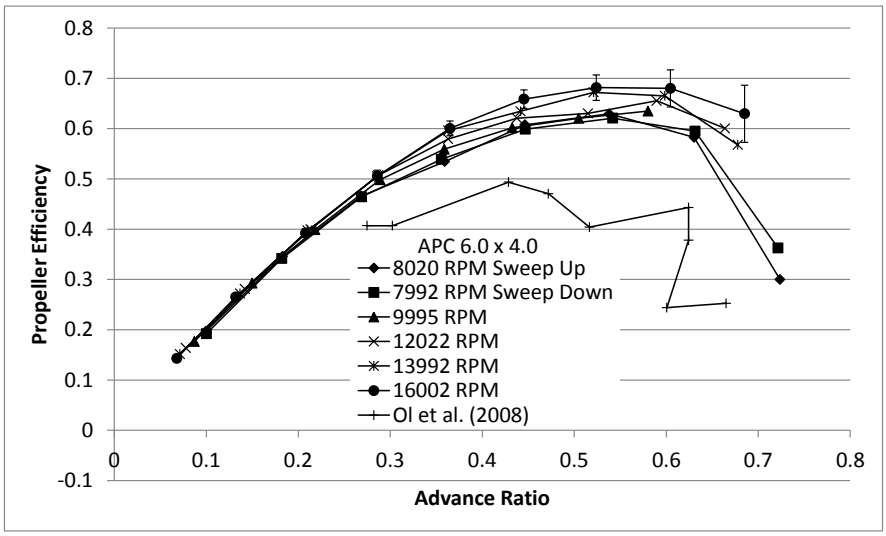

(c)

Figure 10. Comparison of Present Results to Ol et al.[6] (APC 6.0 × 4.0): (a) Dynamic Coefficient of Thrust, (b) Dynamic Coefficient of Torque, (c) Propeller Efficiency.

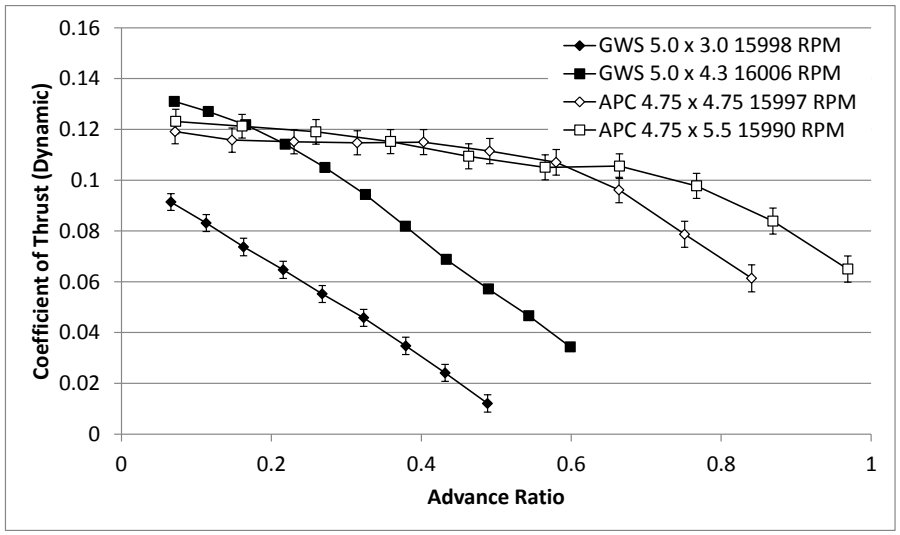

(a)

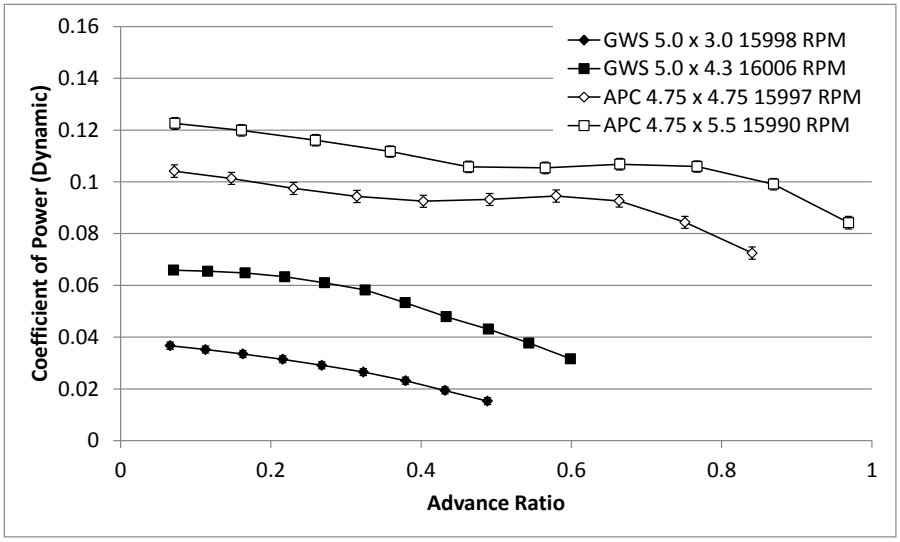

(b)

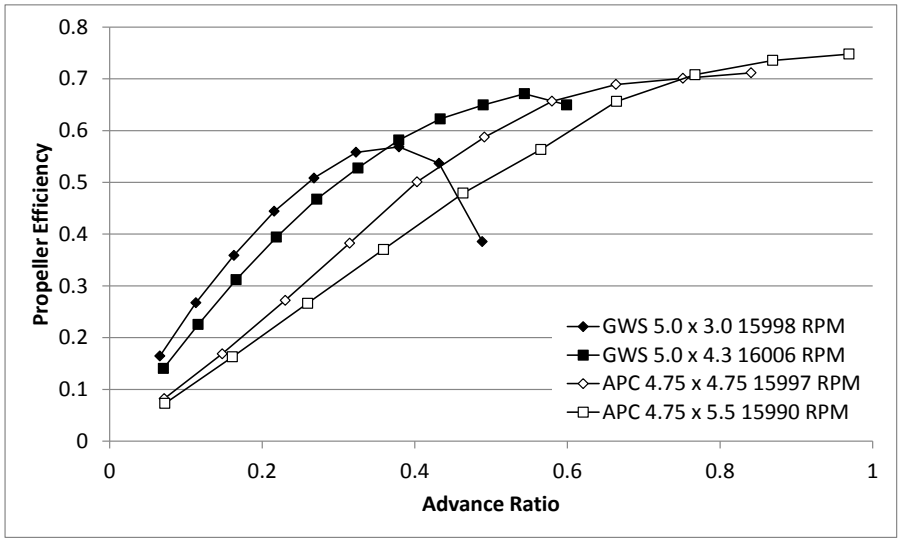

(c)

Figure 11. The Effect of Varying Propeller Pitch While Holding Diameter Constant: (a) Dynamic Coefficient of Thrust, (b) Dynamic Coefficient of Power, (c) Propeller Efficiency.

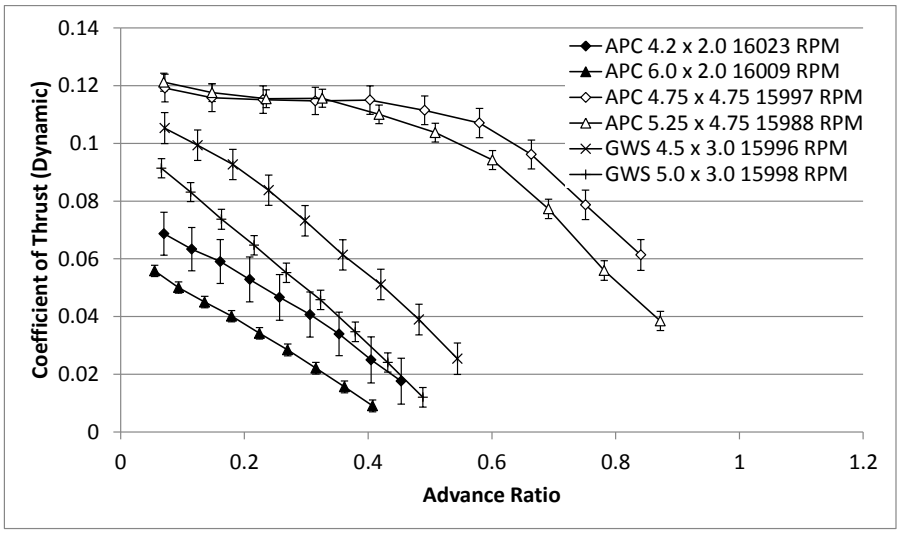

(a)

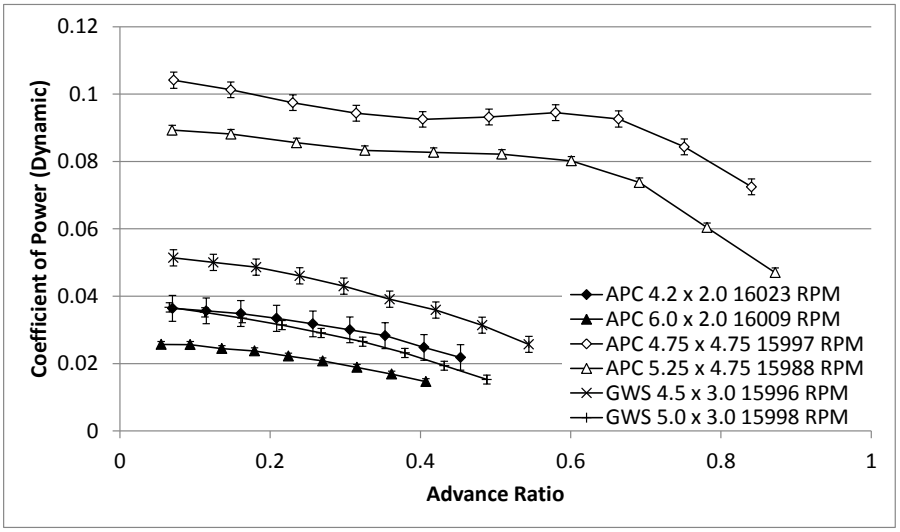

(b)

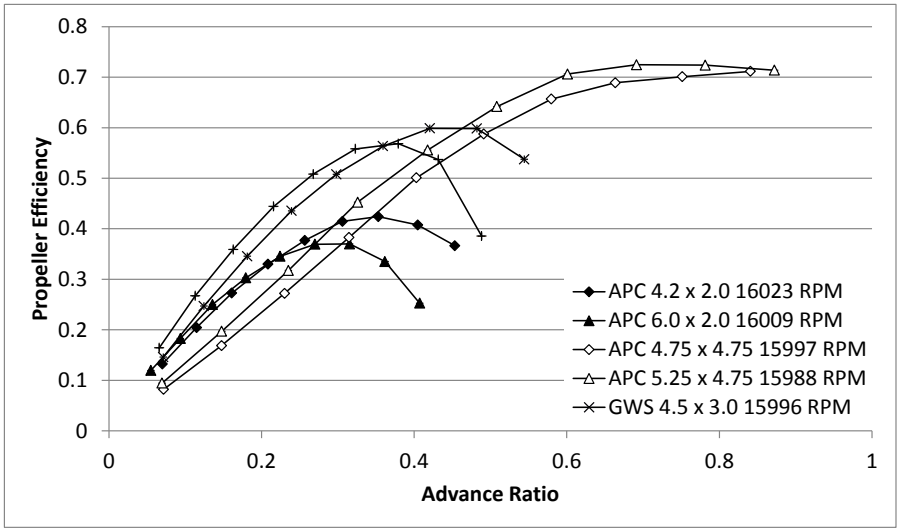

(c)

Figure 12. The Effect of Varying Propeller Diameter While Holding Pitch Constant: (a) Dynamic Coefficient of Thrust, (b) Dynamic Coefficient of Power, (c) Propeller Efficiency.

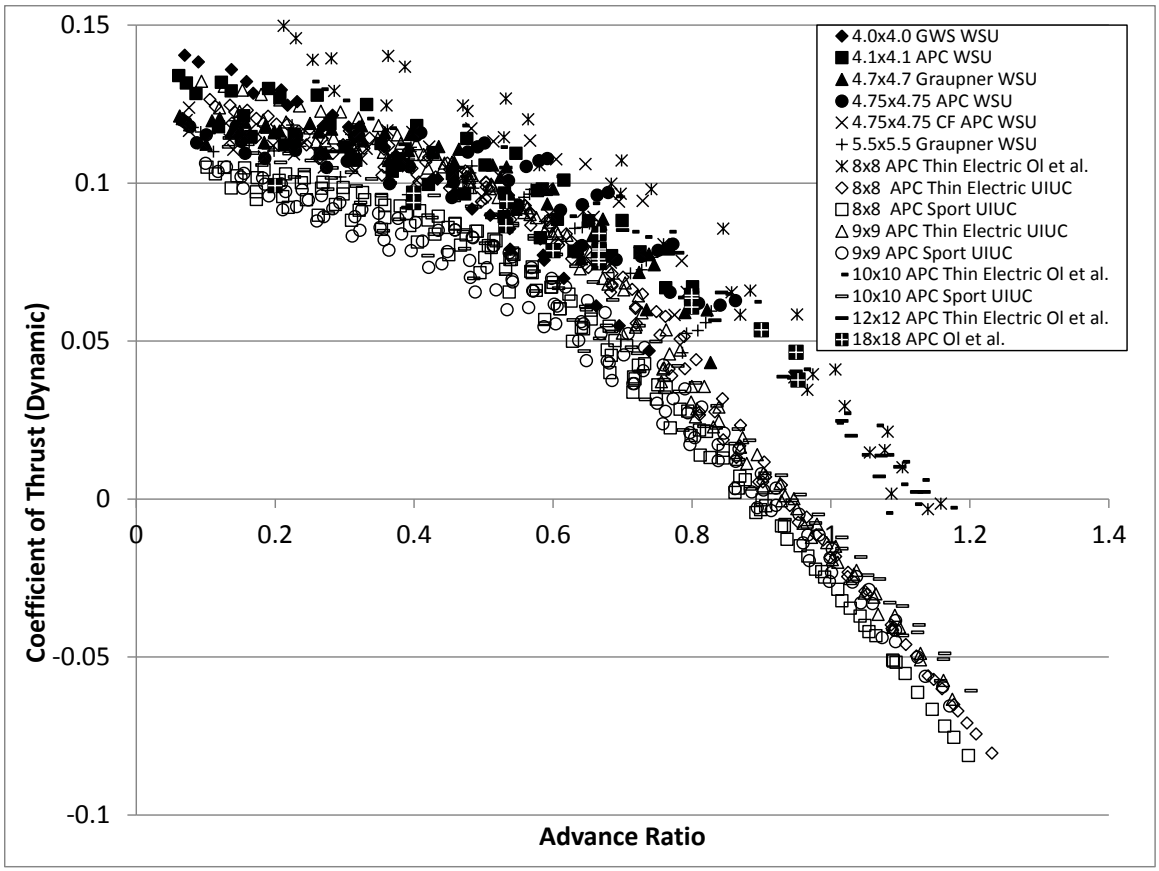

Figure 13. Coefficient of Thrust Versus Advance Ratio for Square Propellers (D/P = 1.0) with Diameter Ranging from $4.0 \leq D \leq 18$ inches.

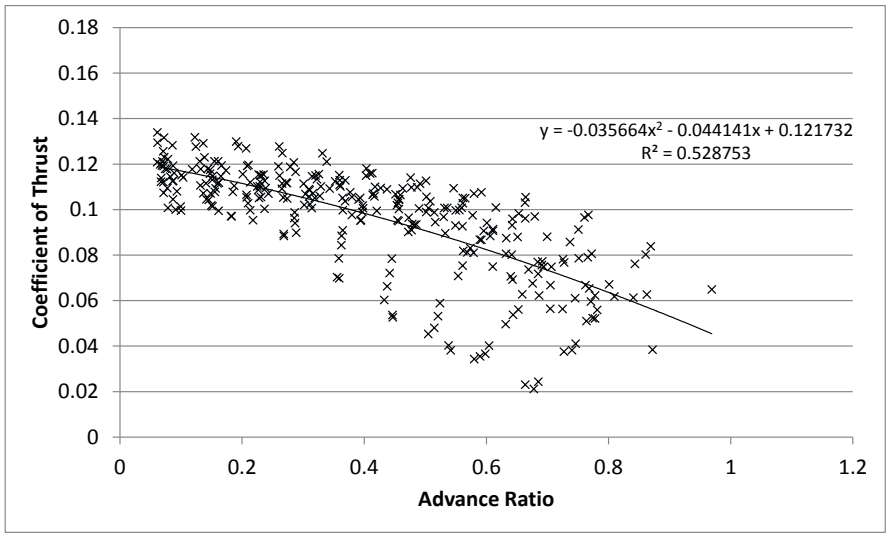

(a)

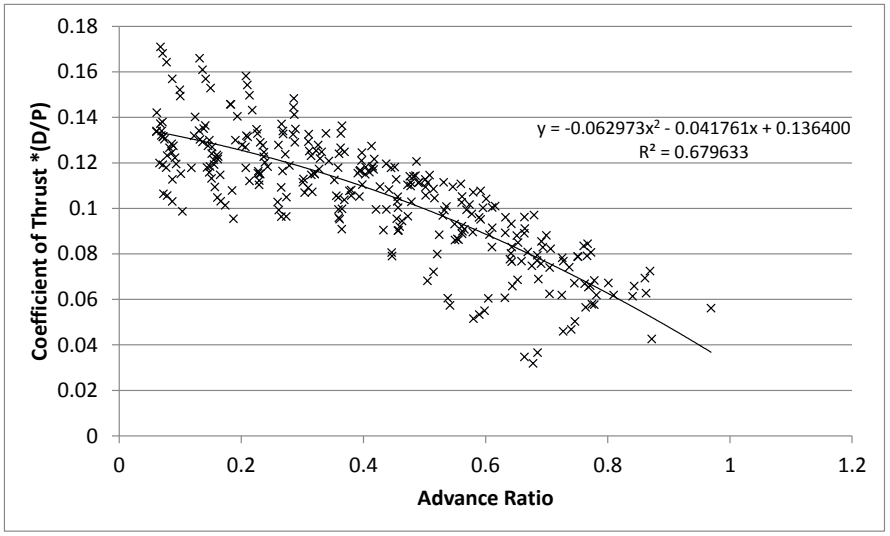

(b)

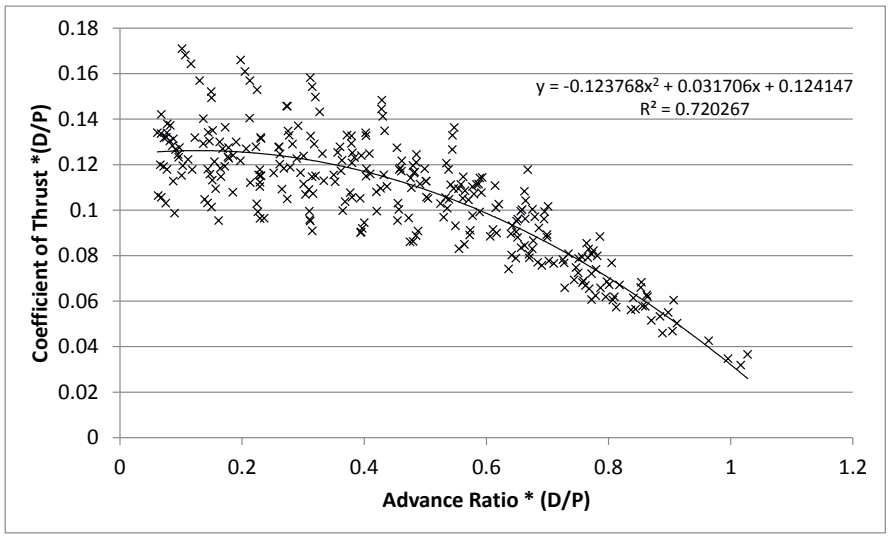

(c)

Figure 14. Coefficient of Thrust Versus Advance Ratio for the APC Sport 400 Electric Propellers ($\Delta C_T \leq$ 20%): (a) Original Representation of C_T; (b) C_T Modified by the Diameter to Pitch Ratio, (c) C_T and J Modified by the Diameter to Pitch Ratio

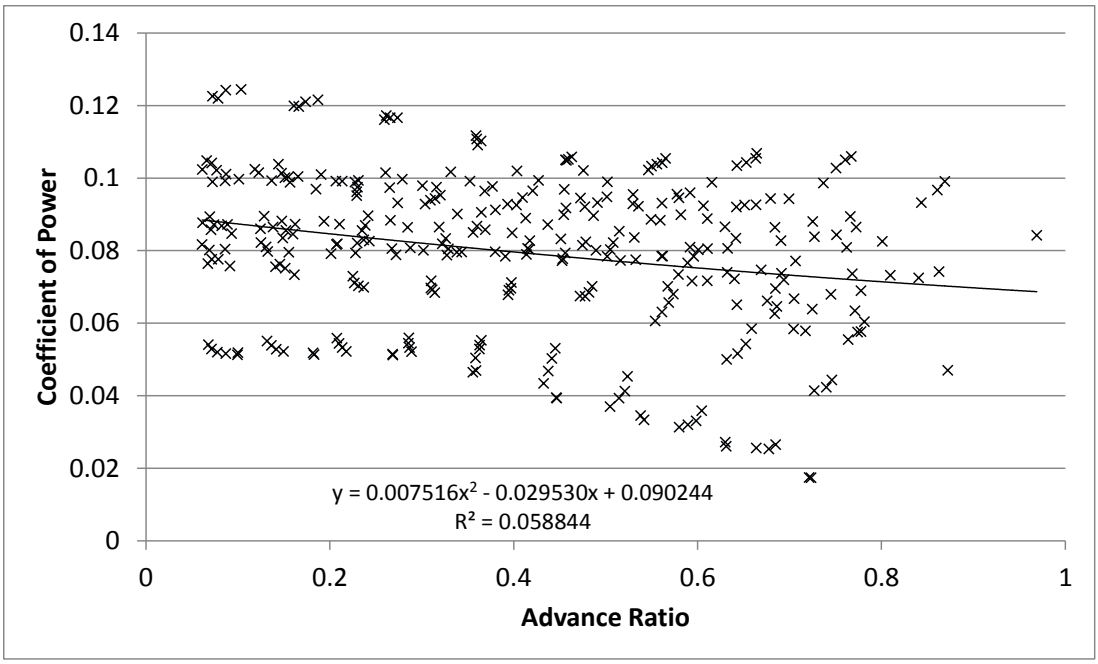

(a)

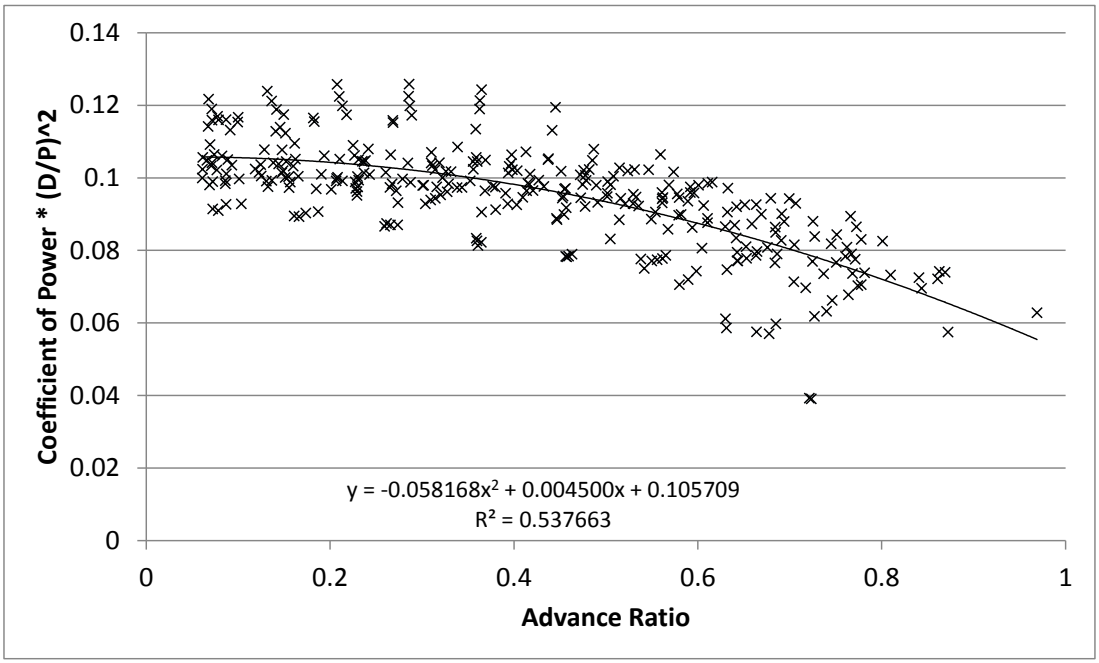

(b)

Figure 15. Coefficient of Power Versus Advance Ratio for the APC Sport 400 Electric Propellers ($\Delta C_P \leq$ 20%): (a) Original Representation of C_P; (b) C_P Modified by the Diameter to Pitch Ratio.

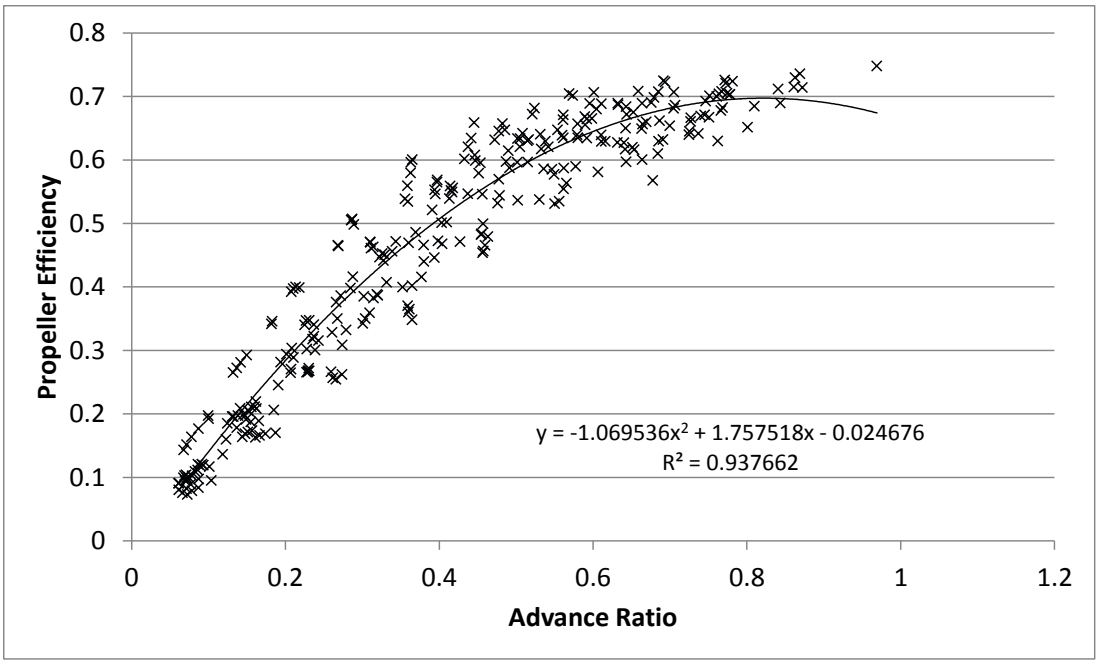

(a)

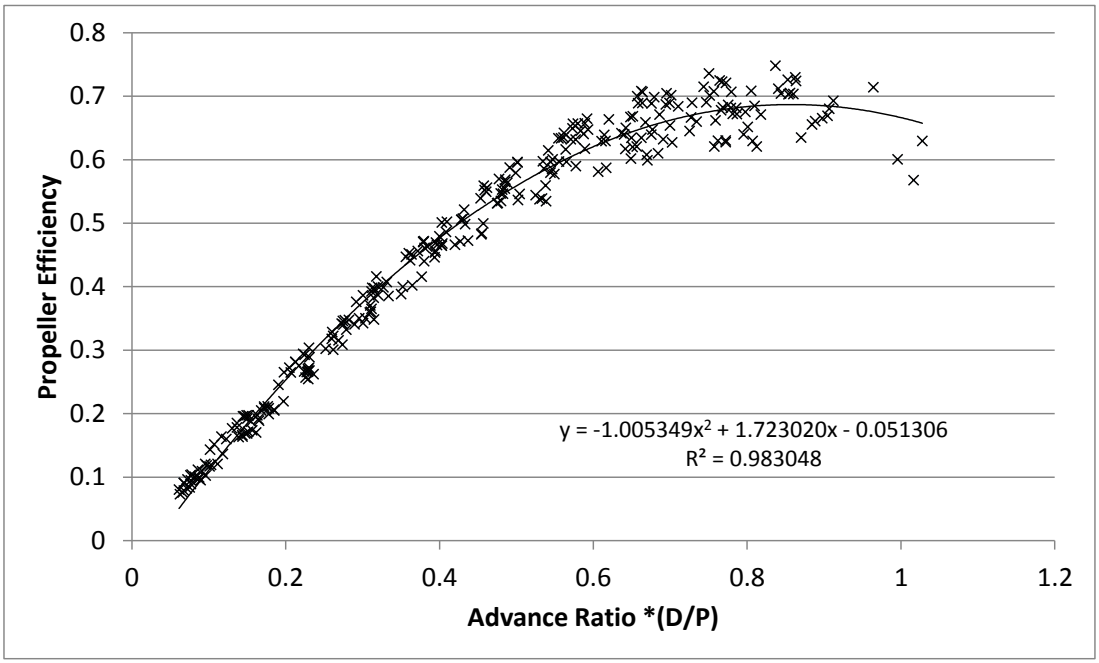

(b)

Figure 16. Propeller Efficiency Versus Advance Ratio for the APC Sport 400 Electric Propellers ($\Delta\eta_P \leq$ 20%): (a) Original Representation of η_P; (b) Advance Ratio Modified by the Diameter to Pitch Ratio.

Table 1. Uncertainties of Primary Measurement Devices and Calibration Sources.

Variable	Measurement Device	Uncertainty
Thrust, T	Transducer Techniques LSP 1kg Load Cell	$\Delta T_{cal} = \pm 7.70$ g
Torque, Q	Transducer Techniques RTS 25 oz-in Reaction Torque Sensor	$\Delta Q_{cal} = \pm 0.0498$ g-m
Atmospheric Temperature, T_{atm}	Omega Type E Thermocouple	$\Delta T_{atm,cal} = \pm 0.0334$ °C
Calibration Mass	Ohaus Digital Scale	$\Delta m = \pm 1.00 \times 10^{-3}$ g
Propeller Diameter, D	Digital Vernier Calipers	$\Delta D = \pm 1.00 \times 10^{-5}$ m
Propeller Chord Length at 75% Radius, $C_{0.75}$	Digital Vernier Calipers	$\Delta C_{0.75} = \pm 1.00 \times 10^{-5}$ m
Propeller Rotational Speed, n	Monarch Instruments Remote Optical Sensor (ROS) and ACT 3x Panel Tachometer	$\Delta n = \pm 1$ RPM
Motor Voltage, V	National Instruments USB-4065 Digital Multi-Meter	$\Delta V = \pm 1.00 \times 10^{-3}$ V
Motor Current, I	CR Magnetics CR5210-30 Current Transducer	$\Delta I = \pm$ (1% × Reading)
Atmospheric Pressure, P_{abs}	Vaisala PTB110 Barometer	$\Delta P_{atm} = \pm 30.0$ Pa
Pitot Tube Differential Pressure, P_{diff}	MKS 226A Differential Pressure Manometer	$\Delta P_{diff} = \pm$ (0.3% × Reading)

Table 2. Summary of Propeller Measurements.

Manufacturer	Nominal *D*/*P* (in × in) (mm × mm)	Propeller Number	*D* (mm)	$R_{75\%}$ (mm)	$C_{75\%}$ (mm)
APC	4.10 × 4.10 Speed 400 Electric (104.1 × 104.1)	1	103.62	38.86	8.09
		2	103.65	38.87	8.09
		3	103.67	38.88	8.11
		Average	103.65	38.87	8.10
APC	4.20 × 2.00 Sport (106.7 × 50.8)	1	105.78	39.67	8.76
		2	105.81	39.68	8.65
		3	105.79	39.67	8.67
		Average	105.79	39.67	8.69
APC	4.20 × 4.00 Free Flight (106.7 × 101.6)	1	106.21	39.83	8.82
		2	106.60	39.98	8.76
		3	106.18	39.82	8.76
		Average	106.33	39.88	8.78
APC	4.50 × 4.10 Speed 400 Electric (114.3 × 104.1)	1	113.95	42.73	8.65
		2	113.89	42.71	8.55
		3	113.80	42.68	8.62
		Average	113.88	42.71	8.61
APC	4.70 × 4.25 Speed 400 Electric (119.4 × 108.0)	1	120.31	45.12	8.45
		2	120.27	45.10	8.42
		3	120.02	45.01	8.39
		Average	120.20	45.08	8.42
APC	4.75 × 4.75 Speed 400 Electric (120.7 × 120.7)	1	120.12	45.05	8.16
		2	119.91	44.97	8.28
		3	119.58	44.84	8.14
		Average	119.87	44.95	8.19
APC	4.75 × 5.50 Speed 400 Electric (120.7 × 139.7)	1	119.87	44.95	8.00
		2	119.90	44.96	8.03
		3	119.99	45.00	8.29
		Average	119.92	44.97	8.11
APC	5.10 × 4.50E Thin Electric (129.5 × 114.3)	1	129.37	48.51	15.17
		2	129.39	48.52	15.27
		3	129.44	48.54	15.29
		Average	129.40	48.52	15.24
APC	5.25 × 4.75 Speed 400 Electric (133.4 × 120.7)	1	132.75	49.78	9.33
		2	132.65	49.74	9.30
		3	132.79	49.80	9.32
		Average	132.73	49.77	9.32
APC	5.50 × 2.00 Free Flight (139.7 × 50.8)	1	139.30	52.24	9.78
		2	139.21	52.20	9.81
		3	139.23	52.21	9.84
		Average	139.25	52.22	9.81

Table 3. Summary of Propeller Measurements, cont.

Manufacturer	Nominal D/P (in × in) (mm × mm)	Propeller Number	D (mm)	$R_{75\%}$ (mm)	$C_{75\%}$ (mm)
APC	5.50 × 4.50 Speed 400 Electric (139.7 × 114.3)	1	139.30	52.24	9.60
		2	139.46	52.30	9.53
		3	139.47	52.30	9.55
		Average	139.41	52.28	9.56
APC	6.00 × 2.00 Sport (152.4 × 50.8)	1	152.25	57.09	8.69
		2	152.19	57.07	9.06
		3	152.14	57.05	8.87
		Average	152.19	57.07	8.87
APC	6.00 × 4.00 E Speed 400 Electric (152.4 × 101.6)	1	152.09	57.03	10.35
		2	151.74	56.90	10.26
		3	151.83	56.94	10.51
		Average	151.89	56.96	10.37
APC	8.00 × 3.8 Slow Flyer (203.2 × 96.5)	1	203.65	76.37	20.79
Graupner	4.00 × 3.00 Cam Speed (101.6 × 76.2)	1	99.77	37.41	9.60
		2	100.06	37.52	9.40
		3	99.94	37.48	9.38
		Average	99.92	37.47	9.46
Graupner	4.70 × 4.00 Cam Speed (119.4 × 101.6)	1	119.16	44.69	9.47
		2	119.16	44.69	9.49
		3	118.96	44.61	9.39
		Average	119.09	44.66	9.45
Graupner	4.70 × 4.70 Cam Speed (119.4 × 119.4)	1	120.22	45.08	8.96
		2	120.22	45.08	8.95
		3	120.49	45.18	9.01
		Average	120.31	45.11	8.97
Graupner	5.50 × 4.30 Cam Speed (139.7 × 109.2)	1	141.11	52.92	10.58
		2	141.08	52.91	10.42
		3	141.13	52.92	10.52
		Average	141.11	52.92	10.51
Graupner	5.50 × 5.50 Cam Speed (139.7 × 139.7)	1	139.60	52.35	9.82
		2	140.37	52.64	9.97
		3	140.17	52.56	9.91
		Average	140.05	52.52	9.90
GWS	4.00 × 2.50 (101.6 × 63.5)	1	101.57	38.09	12.39
		2	101.57	38.09	12.34
		3	101.53	38.07	12.40
		Average	101.56	38.08	12.38

Table 4. Summary of Propeller Measurements, cont.

Manufacturer	Nominal *D*/*P* (in × in) (mm × mm)	Propeller Number	*D* (mm)	$R_{75\%}$ (mm)	$C_{75\%}$ (mm)
GWS	4.00 × 4.00 (101.6 × 101.6)	1	101.98	38.24	10.38
		2	102.00	38.25	10.44
		3	101.99	38.25	10.48
		Average	101.99	38.25	10.43
GWS	4.50 × 3.00 (114.3 × 76.2)	1	114.32	42.87	11.09
		2	114.26	42.85	10.71
		3	114.28	42.86	10.77
		Average	114.29	42.86	10.86
GWS	5.00 × 3.00 (127.0 × 76.2)	1	127.23	47.71	12.43
		2	127.16	47.69	12.36
		3	127.16	47.69	12.39
		Average	127.18	47.70	12.40
GWS	5.00 × 4.30 (127.0 × 109.2)	1	126.89	47.58	12.69
		2	126.83	47.56	12.53
		3	127.03	47.64	12.51
		Average	126.92	47.59	12.58

Acknowledgments

The authors would like to acknowledge the support of the Air Force Research Laboratory through the Joint WSU/AFRL Center for Advanced Power and Energy Conversion Research (CAPEC). In particular, the guidance of Mr. Michael Rottmayer and Dr. Ryan Miller is appreciated.

References

[1]Brandt, J.B. and Selig, M.S. "Propeller Performance Data at Low Reynolds Number." *49th AIAA Aerospace Sciences Meeting.* 2011. AIAA 2011-1255.

[2]Selig, M. *UIUC Propeller Database.* 2012. http://www.ae.illinois.edu/m-selig/props/propDB.html.

[3]Gamble, D.E. "Automated Dynamic Propeller Testing at Low Reynolds Numbers." *M.S. Thesis.* Oklahoma State University, Stillwater, OK, 2009.

[4]Deters, R.W. and Selig, M.S. "Static Testing of Micro Propellers." *26th AIAA Applied Aerodynamics Conference.* 2008. AIAA 2008-6246.

[5]Hepperle, M. *PropellerScanner Software.* 2003. http://www.mh-aerotools.de/.

[6]Ol, M., Zeune, C., and Logan, M. "Analytical – Experimental Comparison for Small Electric Unmanned Air Vehicle Propellers." *26th AIAA Applied Aerodynamics Conference.* 2008. AIAA 2008-7345.

[7]Corrigan, E.K. and Altman, A. "Survey of Small Unmanned Aerial Vehicle Electric Propulsion Systems." *46th AIAA Aerospace Sciences Meeting.* 2008. AIAA 2008-179.

[8]Glauert, H.. *The Elements of Aerofoil and Airscrew Theory.* Cambridge: Cambridge University Press, 1926.

[9]Hackett, J.E., Lilley, D.E., and Wilsden, D.J. *Estimation of Tunnel Blockage from Wall Pressure Signatures: A Review and Data Correlation* . NASA CR15-2241, 1979.

[10]Merchant, M.P. and Miller, L.S. "Propeller Performance Measurement for Low Reynolds Number UAV Applications." *44th AIAA Aerospace Sciences Meeting.* 2006. AIAA 2006-1127.

[11]Selig, M., and Ananda, G. *Low Reynolds Number Propeller Performance Data: Wind Tunnel Corrections for Motor Fixture Drag.* 2011. http://www.ae.illinois.edu/m-selig/props/uiuc-props-wind-tunnel-correction.pdf.

[12]NACA. *Equations, Tables, and Charts for Compressible Flow, NACA Report 1135.* Washington, D.C.: U.S. Government Printing Office, 1953.

[13]Brezina, A. "Measurement of Static and Dynamic Performance Characteristics of Electric Propulsion Systems" *M.S. Thesis.* Department of Mechanical and Materials Engineering, Wright State University, Dayton, OH, 2012.